Univerzita Karlova v Praze

Přírodovědecká fakulta

Ústav geologie a paleontologie

Studijní program: Geologie

Studijní obor: Geologie

Bc. Magdalena Hrnková

Záznam změn mořské hladiny, cirkulace a disperze sedimentu v hemipelagitech svrchního turonu české křídové pánve

The record of sea-level changes, water circulation and sediment dispersion in the Upper Turonian hemipelagic strata of the Bohemian Cretaceous Basin

DIPLOMOVÁ PRÁCE

Vedoucí diplomové práce Mgr. Jiří Laurin, Ph.D.

Konzultanti diplomové práce:

prof. RNDr. František Hrouda, CSc.

RNDr. David Uličný, CSc.

RNDr. Tomáš Matys Grygar, Ph.D.

Praha, 2013

Disclaimer:

I certify that the thesis I am submitting is all my own original work, and that I have made appropriate references to any sources used. I confirm that I have read and understood the University's rules relating to plagiarism. This work has not been previously submitted to any other academic institution.

Prague, 12.8.2013

Prohlášení:

Prohlašuji, že jsem závěrečnou práci zpracovala samostatně a že jsem uvedla všechny použité informační zdroje a literaturu. Tato práce ani její podstatná část nebyla předložena k získání jiného nebo stejného akademického titulu.

V Praze, 12.8.2013

Podpis / Signature .....

Acknowledgements

Firstly, I would like to thank my family for their support, without which I would have struggled to have done any of this.

This research is a part of a Master's Degree Project at Charles University in Prague. It was funded by a Student Research Grant from the Society for Sedimentary Geology and undertaken as a research core funded by the Grant Agency of the Czech Republic (No. P210/10/1991), Principal Investigator RNDr. David Uličný, CSc.

My thanks go to him, not only for allowing me to work on the drill core but also for consulting and providing me with advice. I am particularly grateful for the field work experience, which has helped me to gain a better understanding of the geological background and sedimentary record in the area. He kindly allowed me to incorporate the newest research results to compare with my conclusions; from a team of authors. Kate Olde kindly performed the palynolomorph investigation on additional six samples for the purpose of this thesis.

Thanks to Prof. RNDr. František Hrouda CSc. for being my second consultant who provided me with many insightful comments and discussions on the intricacies of scientific work. He and RNDr, Marta Chlupáčová, CSc. substantially helped with the MS data collection, providing instructions and guidance as well as comments on possible interpretations.

Thanks to Mgr. Leona Koptíková, Ph.D., Doc. RNDr. František Holub, CSc. and RNDr. Helena Klápová, CSc. who provided invaluable advice on micropetrology and Doc. RNDr. Katarína Holcová, CSc. whom I consulted on foraminifera and Mgr. Stanislav Čech who provided information on stratigraphy.

I would also like to thank Mgr. Viktor Goliáš, Ph.D. for providing the tools for preparing geochemistry samples and Mgr. Karel Martínek, Ph.D. for the use of the camera lighting equipment, literature and also for his time in helping me to assess the thin sections.

I am thankful to the company AGICO s.r.o. for allowing the use of the MFK1-FA Kappabridge and to the company Georadis s.r.o. for providing the KT-10 Kappameter. Thanks to both Charles University and the Academy of Sciences who made the microscopes and cameras available for use. Thanks to the Lafarge cement Co who allowed me access to their property.

And the final thank you, which is the most important one, goes to my supervisor Mgr. Jiří Laurin, Ph.D. (Geophysical Institute, Academy of Sciences of the Czech Republic) for offering an interesting subject to work on. His ongoing interest and instruction kept this thesis on track as well as providing motivation. He provided me with the essential time-series analysis software but most importantly shared his many years of experience on their usage. He also allowed the full use of some of his unpublished work and supplied comments on the applied methods. His suggestions were used to significantly improve the manuscript. Some of the most valuable lessons and skills necessary for further scientific work were learnt from him.

Contents

1 Introduction

The Late Cretaceous Epoch is an interval in the Earth's history characterised by distinct climatic and oceanographic conditions (*for review see e.g. Hay and Floegel, 2012*) The greenhouse climate driven by extremely high pCO_2 levels (*e.g. Bice et al., 2006*) was culminating during the Cenomanian and Lower Turonian (*e,g, Hu et al., 2012*). The long-term change in the strontium isotope record suggests a deceleration of volcanic activity by the Late Turonian (*Jones and Jenkyns, 2001*). Perturbations in the carbon cycle are indicated by carbon-isotope events such as the positive Hitch Wood Event and the negative Navigation Event (*e.g. Jarvis et al., 2006*). A reorganisation of climate belts, possibly connected to the changes in atmospheric circulation, was documented in terrestrial as well as marine records (*Sokolova, 2009; Hasegawa et al., 2011*). In Europe the combination of sea level highstand and the reactivation of tectonic processes resulted in the juncture of the Northern Atlantic with Tethys (*Ziegler, 1990*) and enabled the migrations of Boreal Fauna some of which coincides with the cooling documented by the $\delta^{18}O$ excursions (*Voigt & Wiese, 2000*). The causal relationships between the different lines of investigation are not yet fully understood and further research is necessary to unveil the processes connecting these individual observations.

The Bohemian Cretaceous Basin was positioned at a crucial paleogeographic location between the two paleobiogeographic provinces (*Wiese et al., 2004*). As a shallow marine epicontinental strait, it was especially suited to the preservation of both hemipelagic and nearshore deposits, allowing for the study of the complex interplay between tectonics, eustatic sea level changes and paleoceanographic conditions (*Laurin & Uličný, 2004*, *Uličný et al., 2009*). A further investigation into the preserved Milankovitch frequency lithology variations and secular events, such as the onset of hemipelagic sedimentation in Late Turonian, could bring invaluable information to the general picture.

The aim of this thesis is to perform a comprehensive study of the Upper Turonian record in Bch-1 core, located in the central part of the basin, and its integration with current knowledge of equivalent deposits in the south-western part of the Bohemian Cretaceous Basin. A detailed lithologic investigation and multi-proxy approach is used to explore the core succession marked by recurrent carbonate beds. Element ratios, carbonate content, grayscale and magnetic susceptibility data were gathered and they

will be interpreted in order to identify the origin of these lithological variations; especially their relation to siliciclastic input, biologic productivity and the changes in sea level were addressed. One of the main objectives is to determine the periodic character of lithological variability through the use of high-resolution datasets and ascertain their possible link to insolation variability. The information gained from the core investigation will then be used to hypothesize on circulation and dispersion of the sediment during the deposition of coeval Teplice Formation hemipelagites.

The results should cast new light upon the origin of carbonate rhythmicity in Upper Turonian hemipelagic deposits of Bohemian Cretaceous Basin and contribute to the efforts on isolating global climatic signals within these successions.

2 Overview

2.1 Late Cretaceous World

The Late Cretaceous World was very different to the one we are used to now; with a very warm Greenhouse climate with distinct paleogeography and the characteristic sediments that make it one of the most puzzling intervals of geological history.

Large areas of land were flooded during the Late Cretaceous as a consequence of the globally high sea level (*e.g. Haq et al., 1988*), a result of the from elevated spreading rate of the mid-ocean ridges and the itra-oceanic plateau volcanism (*e.g. Larson, 1991*). This long-term rise is estimated to have peaked at 100 ± 50 m above curent sea level (*Miller et al., 2005*). A number of Cretaceous transgressions have been reported from various basins worldwide and their intercorrelation is used to show the global eustasy signal (*Hancock & Kauffman, 1979*). The buoyant ridges, displacing seawater onto a continent, (*Ziegler, 1990*) could certainly be held responsible for the global highstand, yet some superimposed fast and abrupt changes in the sea level, which occurred during the Late Cretaceous, has repeatedly been proposed to have been controlled by glacioeustasy (*Miller et al., 2010*).

The rise in sea level facilitated reopening of seaways and linked the previously separated faunal provinces; the colder-water Arctic, West Siberian platform and Barens Shelf have been linked with the warmer North and Central Atlantic oceans and the Tethys Sea (*Ziegler, 1990*). The sedimentological evidence from the Anglo-Paris Basin, Lower Saxony Basin and the North Cantabrian Basin documents the relationship between the low-order transgression and the southward drift of the northern taxa , which suggests a regional control. (*Voigt & Wiese, 2000*) and there are certain indices that the local shifts of Boreal and Tethyan faunas were a part of a larger global scale shift in climatic zones (*Sokolova, 2009*) possibly laying poleward and equatorward of the subtropical fronts (*Hay, 2008*).

A new unique lithofacies type, chalk, was deposited over large areas of Western and Central Europe (*Ziegler, 1990*), these relatively cold water pelagic carbonates are similar to modern deep-sea nannoplankton ooze but deposited in an intracontinental environment (*Hay, 2008)*

Another unusual phenomenon was the occurrence of global ocean anoxic events (OAE 2), which is marked by the presence of pelagic black, organic shales (*Schlanger*

& Jenkyns, 1976) OAE, occurring at Cenomanian-Turonian boundary, and its mechanism is being extensively studied ever since uncovering by the Deep Sea Drilling Project (*Schlanger & Jenkyns,1976; Erba 2004*). $\delta^{18}O$ has also displaed a decrease over the Cenomanian-Turonian anoxic event (*Jones & Jenkyns, 2001*) and highlights its usefulness as a temperature proxy even in the Late Cretaceous world (*Miller et al., 2010*).

Cretaceous biostratigraphy and the isotope $\delta^{13}C$ record are aided by other independent stratigraphic tools such as the isotope $^{87}Sr/^{86}Sr$ ratio and magnetic stratigraphy, allowing a global correlation (*Voigt et al., 2008*). A distinct, relatively short-term minimum in the $^{87}Sr/^{86}Sr$ ratio occurred during the Cenomanian to Santonian and was attributed to increased hydrothermal activity (*Jones & Jenkyns, 2001*).

2.1.1 Climate

The Cretaceous climate is often described as warm and equable, suggesting a mild uniform climate (*Francis & Frakes, 1993*) and it is true that this period was the climax of the Mesozoic Greenhouse (*e.g. Friedrich et al., 2012*). As seen from the paleorecontructions of Chumakov et al. 1995 (*Hay & Floegel, 2012*) the general expansion of climate belts towards high latitudes was present. Faunas and floras typical inr warm climates spread into the high latitudes and the climate sensitive rocks signalled humid conditions (*Francis & Frakes, 1993*). Moreover, the equator to pole temperature gradient is expected to have been lower (*Hasegawa et al., 2011*).

It has been proposed that the Greenhouse climate is linked to the high CO_2 levels in the atmosphere (*e.g. Francis & Frakes, 1993, Bice et al., 2006*). Kidder and Worsley in 2012 introduced the two states of the Greenhouse and a Hothouse in order to efficiently describe the different states of Earth; the Late Cretaceous would fall into the Warm Greenhouse with a global average temperature between 24 and 30 degrees and possibly the Hothouse during the OAE 2 (*Hay & Floegel, 2012*).

A similarity in temperature trends is quite consistent worldwide, however the climate has been variable rather than stable (*Francis & Frakes, 1993*) and the warmest conditions were indicated for the Cenomanian and Turonian (*e.g. Hu et al., 2012*). This climax in Early Turonian is in agreement with the observations of Voigt and Wiese (*2000*), who described Late-Middle Turonian as a time of relative climatic cooling; this

cooling would have been accompanied by a southward shift of cooler water masses in Europe and was interpreted as a water circulation reorganization (*Voigt & Wiese, 2000*).

The Greenhouse climate is considered to have been different as the termohaline circulation is expected to have been slow (*Hay & Floegel, 2012*). One of the possible explanations has been a frequent reversal of the atmospheric pressure system, accompanied by the changing direction of westerly winds; weak and unstable winds would have caused a breakdown of the ocean circulation and its replacement with less well-organised mesoscale eddies (*Hay, 2008*).

Generally, as the Earth warms, the Hadley circulation expands (*Hay & Floegel, 2012*). These expected shifts in the subtropical high-pressure belt were confirmed by Hasegawa et al. (*2011*) based on observations in the distributions of desert deposits in the Asian interior; they have postulated the poleward expansion of Hadley circulation cell during the Early and Late Cretaceous and an episode of drastic shrinkage during the mid Cretaceous. The result of such reorganisation of global importance would have caused variations in the ocean circulation (*Hasegawa et al., 2011*).

2.1.2 European Platform

The European continental plate was bordered by the North Atlantic Ocean and the Arctic Sea to the north and northwest (*Voigt et al., 2008*). The Arctic sea was much smaller during the Cretaceous and had a relatively low salinity, possibly even freezing over during the polar night (*Hay & Floegel, 2012*). In the North Atlantic sea floor spreading remained active during Cenomanian to early Senonian times (*Ziegler, 1990*), including the Bay of Biscay spreading to the south-west. The north-western branch of the Tethys Ocean laid to the south and the European Platform to the east (*Voigt et al., 2008*)

The long-term Cretaceous sea level rise was punctuated by a high order, mostly eustatic sea-level changes, which were responsible for the repeated flooding and retreat of the sea (*Uličný et al., 2009*). The Cenomanian was a period of major continuous and progressive transgression and a minor regressive phase occurred in the mid-Turonian; the Latest Turonian was generally mildly regressive (*Tyson & Funnell, 1987*). The marine sedimentation continued until the Maastrichtian but the general trend of regression started back in Santonian (*Hancock & Kauffman, 1979*). In western and central Europe the rising sea level combined with regional subsidence which resulted in a progressive overstepping of basin margins (*Ziegler, 1990*).

The alpine collision of the Italo-Dinarid block with the southern margin of Europe, was accompanied by a gradual build-up of compressional stress that caused the intraplate deformation and uplift from the Senonian onwards (*Ziegler, 1990*).

2.2 The Bohemian Cretaceous Basin

The Bohemian Cretaceous Basin (BCB) is a Mesozoic sediment accumulation extending over 14,600 square kilometres in the Czech Republic, Saxony and Klodzko, ninety percent of which is situated in the Czech Republic (*Chlupáč, 2002*). The area is elongated with the main axis oriented in a NW-SE direction over the majority of its length. The deposits are preserved in two to four hundred metre successions, with extremes around one thousand metres in the proximity of Děčín (*Herčík et al., 1999*).

The bedrock is made up of crystalline Variscan basement including intrusives, metamorphosed Proterozoic and Paleozoic sediments, as well as Permo-Carboniferous basins and Triassic sediments (*Malkovský, 1974*). The reactivation of the pre-existing shear zones in the Variscan basement during the mid-Cretaceous led to a new accumulation of sediments in this area (*Uličný et al., 2003*). This reactivation has commonly been assigned to far-field stresses of the commencing Alpine orogeny (*Ziegler, 1990*).

The BCB was formed in Albian (*Ziegler, 1990*) or early Cenomanian (*Malkovský, 1987*) and quickly developed into a shallow-water epicontinental seaway by means of the local transtensional normal faulting and global sea level rise (*Uličný & Špičáková, 1996*). Such an interplay of the global and local signal is typical throughout the BCB history (*Uličný et al., 2009*), which is especially important when trying to correlate the observed sedimentary developments to other Cretaceous basins and global phenomena. The Cretaceous sea receded again in Santonian as a consequence of tectonic uplift (*Malkovský, 1987*) and the record of BCB terminates in Campanian (*Ziegler, 1990*).

The present state is that of a tectonically reworked basin fill, clearly asymmetric to the NE (*Ziegler, 1990*) with boundaries being mainly erosional and partly tectonic (*Herčík et al., 1999*). The only major cover unit is connected to the tertiary volcanites of České Středohoří and limnic basins in Ohře Graben in the south-west and some Neogene marine sediments in the east; the rest of the sediments are covered with a thin layer of quaternary deposits (*Herčík et al., 1999*).

2.2.1 Stratigraphy

Our understanding of BCB has gradually developed since 1844 when the first attempts on lithostratigraphic classification were made by Reuss (*Wiese et al., 2004*). Many other authors, including Krejčí, Zahálka and Soukup, have developed progressively more sophisticated lithostratigraphic classifications (*Čech et al., 1980*) until new disciplines and practices in biostratigraphy and sequence stratigraphy allowed for further advances in this field.

A formal stratigraphic subdivision of the BCB by Čech et al. (*1980*) is based on the regional lithostratigraphic concept and follows the formerly established rock-stratigraphic concept of Frič (*Čech, 2011*) and it defines six formations (*Čech et al., 1980*). The earliest, the Cenomanian Perucko-Korycanské Formation was geomorphology dependent (*Malkovský, 1974*) and it reflects the progressive sea transgression and transition from fluvial to marine environment (*Uličný & Špičáková, 1996*). Bělohorské, Jizerské and Teplické Formations are defined in the Turonian, which is the focus of this study and will be discussed further in terms of paleoenvironment and the sedimentary record. The overlying Březenské Formation was deposited during the Coniacian and possibly Santonian (*Čech et al., 1980*). The youngest Merboltické Formation is highly eroded and preserved only under a Cenozoic volcanite cover (*Chlupáč, 2002*). Lithofacies in the BCB, however, show pronounced local variations.

Both macrofossils and micro- or nannofossils are used for the biostratigraphic correlation. Foraminiferas, calcareous nannoplankton and palynomorphs have been studied (*for review see Čech, 2011*). The inoceramid bivalve assemblages enable correlations with other basins worldwide (*Čech, 1989; Wiese et al., 2004*) as well as ammonites and several incursions of typical Boreal fauna were accompanied by the occurrence of belemnites (*Košťák, 2004*) Echinoderms, sponges, brachiopods and vertebrates are also studied (*Čech, 2011*). These biostratigraphic correlation techniques can be refined with chemostratigraphic correlation (*e.g. Štaffen, 1999*).

An informal genetic stratigraphy was developed to further divide the basin fill history and is based on a basin-wide correlation of transgressive surfaces; the genetic sequences are derived from clastic deposits of the Lužice-Jizera sub-basin (*Uličný et al., 2009*). This division is especially suited to decoding the transgressional episodes in the basin fill history. As the same correlation tools were used to integrate the studied core

into the whole basinal concept (*Uličný et al., submitted*) the nomenclature will be referenced in this thesis.

Another quickly developing branch is the stable carbon isotope stratigraphy (*Uličný, 1997; Wiese et al., 2004; Uličný et al., submitted)*

2.2.2 Paleogeography and Sediment Source Areas

A vast epicontinental sea covered most of the north-western and Central Europe, see **fig. 2.2-1**, during the mid-Cretaceous (*Chlupáč, 2002*) and formed a group of basins on the tectonically active edge of the European Platform (*Herčík et al., 1999*). The other basins in the proximity were the North Sudetic basin and the Opole basin (*Valečka & Skoček, 1990*).

The BCB formed a shallow strait, located between the two climate belts and biogenic realms, with the Tethyan Realm to the south and Boreal Realm to the north and was repeatedly influenced by the varying extent of immigrations of the two respective cool- and warm-water faunas (*Wiese et al., 2004*) and provided an effective pathway for the water-mass exchange between the Proto-Atlantic Ocean to the west and the closing Neotethys Ocean to the south-east (*Mitchell et al., 2010*).

The importance of the emerging island heights as a source of clastic material was recognised early on. The tectonically active Western Sudetic Island lay to the north-west and the comparably low-relief Central European Island to the south (*Valečka, 1979*), although the explanation for their differential uplift histories was only first satisfyingly explained by the introduction of the transtensional basin model (*Uličný, 2001*). The less influential Eastern Sudetic Island lay to the north-east (*Skoček & Valečka, 1983*). These tectonically active elevations were an effective source of clastic material as well as barriers and constraints on the basin circulation.

Thick sequences of sandstones, typical for BCB, are somewhat anomalous within the mid-European successions and occur only in two regionally limited areas - the BCB and the North Sudetic Basin (*Skoček & Valečka, 1983*), although similar wide clastic coastal belts did occur around the other emergent masses, such as the Armorican Massif and Massif Central or the Irish and Cornubian Massifs (*Mitchell et al., 2010*).

There is no evidence for Mesozoic volcanic activity in the area of the BCB (*Malkovský, 1974*).

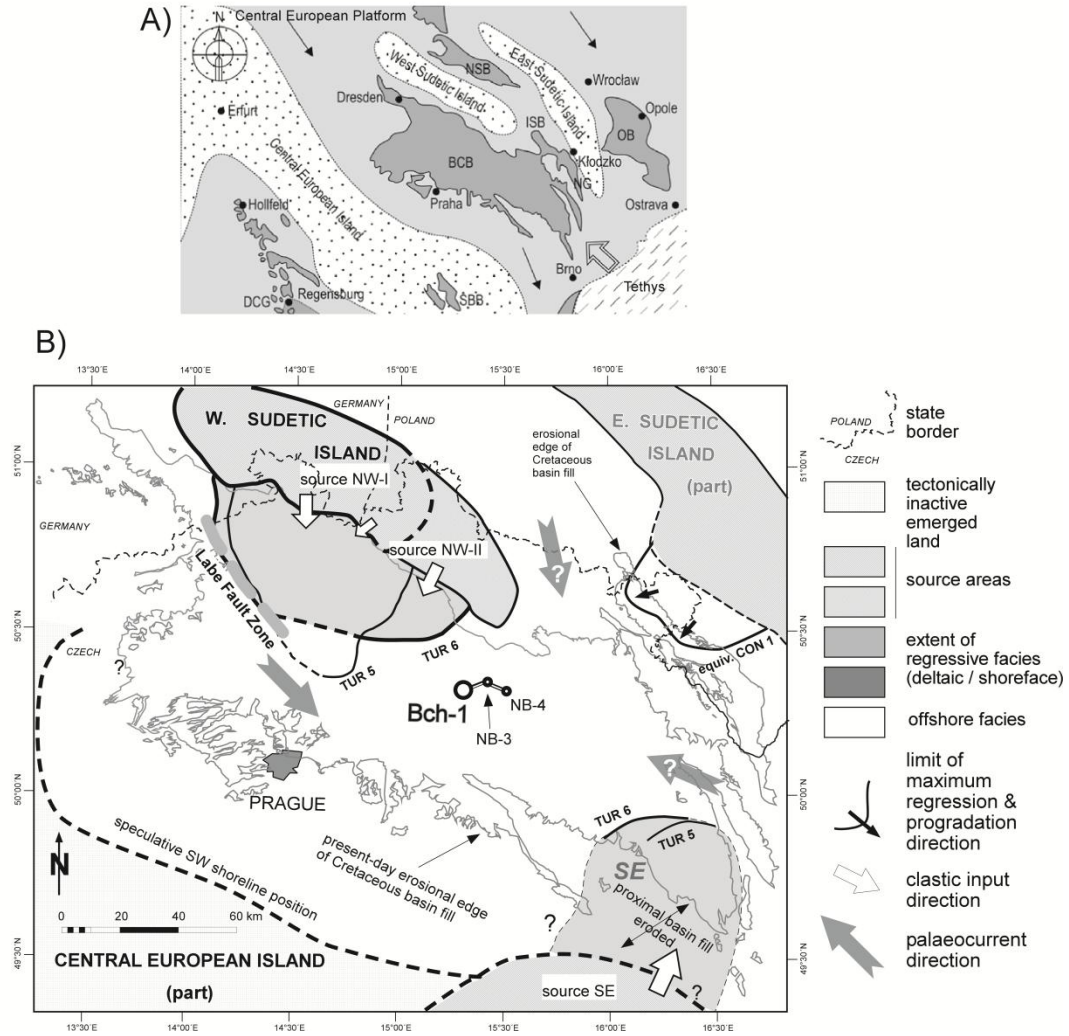

Fig 2.2-1

The two maps show position of the Bohemian Cretaceous Basin, within the Central European platform and adjoining Opole and North Sudetic Basins in picture A) with highlighted position of preserved sedimentary deposits. The shift of main depocentre between TUR 5 and TUR 6 based on new correlations.
A) modified after Čech (2011) B) modified after Uličný et al., submitted and Uličný et al., 2009

2.2.3 Sedimentary Environments

The subsidence rates in the BCB, during the mid-Cretaceous, are expected to have been low, below 110 m/Ma, until the Latest Turonian as inferred from the quantitative subsidence analysis. This water depth did not reach over 100 m in most parts (*Uličný et al., 2009*), and a plentiful sediment supply led to rapid progradation of the coarse clastics into the basin. The two main facies nearshore psamitic and distal aleuropelitic have been recognised (*Valečka, 1979*). Although the sedimentary environment of the coarse siliciclastics deposits remains somewhat disputed and dune migration has been

proposed (*Skoček & Valečka, 1983*), a deltaic sedimentation appears to be more plausible, see discussion in Uličný (*2001*).

The coarse grained lobate deltas passed distally into fine-grained offshore sediments (*Laurin & Uličný, 2004*). Lithologically these successions are dominated by cross-bedded sand stone, with large-scale clinoform geometry (*Uličný et al., 2009*). The spatial facies architecture was controlled by the interplay between sediment supply and relative sea-level change, and this system reacted to such changes with a predictable pattern; the major transgressive surfaces are mappable regionally as gravel lags (*Uličný et al., 2009*).

Many studies also confirm a vigorous current activity (*Skoček & Valečka, 1983; Uličný, 2001*) and numeric models for Early to Middle Turonian predicted microtidal to mesotidal regime with elevated tidal ranges in local embayment's, which would have a direct impact on sediment dispersal and facies distribution (*Mitchell et al., 2010*). Bottom shear stress induced by the tidal currents would have been important for transport of the fine-grained particles (*Uličný et al., 2009*).

Carbonate dominated fine-grained deposits in the offshore realm occur at two stratigraphic levels, in Lower Turonian Bílá Hora Formation and in Upper Turonian Teplice Formation (*Valečka & Skoček 1990*). These sediments are particularly interesting as they provide a wealth of information on ancient paleoceanography and climate (*Laurin & Vodrážka, 2010*).

2.3 Object of Study

The majority of the research was performed on the Bch-1 core. This project was, among other goals, aimed to investigate the transgressive-regressive history of distal hemipelagic facies downstream to the main siliciclastic depocentre in north-west, a question to which this thesis could bring additional information.

The stratigraphy of the core is well ascertained; see **fig. 2.3-1**, through the combined use of biostratigraphy, performed by Mgr. S. Čech, and well-log correlation to other parts of the basin performed by RNDr D. Uličný CSc. and his team, see **appendix 1** for more information on the core.

A great number of geophysical, geochemical and paleontological data were used to investigate the core, some of which were adopted in this thesis for the purpose of multi-proxy approach interpretation. The adopted datasets are the ICP geochemistry, collected

in two metre intervals and the XRF carbonate measurements, collected in one metre intervals. For more details, see part on methodology.

Other data, such as resistivity log, $\delta^{13}C_{org}$ curve, Terrestric to Marine palinomorph ratio and dinoflagelate diversities were used for comparative and correlation purposes. Only a simplistic approach was used with these datasets and is explained in the text when needed.

The interval between 202 m and 145 m was chosen for a more detailed study based on several observations. There was a pronounced increase in siliciclastic input indicators with a variation in geochemistry ratios signalling an unusually dynamic environment (*Uličný et al., submitted*). This observation was confirmed by a brief inspection of the Bch-1 core, documenting thin sections which confirm that the studied interval is by far the most coarse-grained in lithology. At the same time, the lithology displayed obvious rhythmic variations in carbonate content in the form of carbonate rich, distinctly light coloured beds.

Based on these observations and the fact that in other parts of the basin positioned perpendicular to the main current directions (for example in the Úpohlavy quarry and sections in Kystra and Lenešice) this geological interval displays a very characteristic development (*Wiese et al., 2004*), including Milankovitch band cyclicity (*Laurin & Uličný, 2004*) a comparison to the along shore development was proposed.

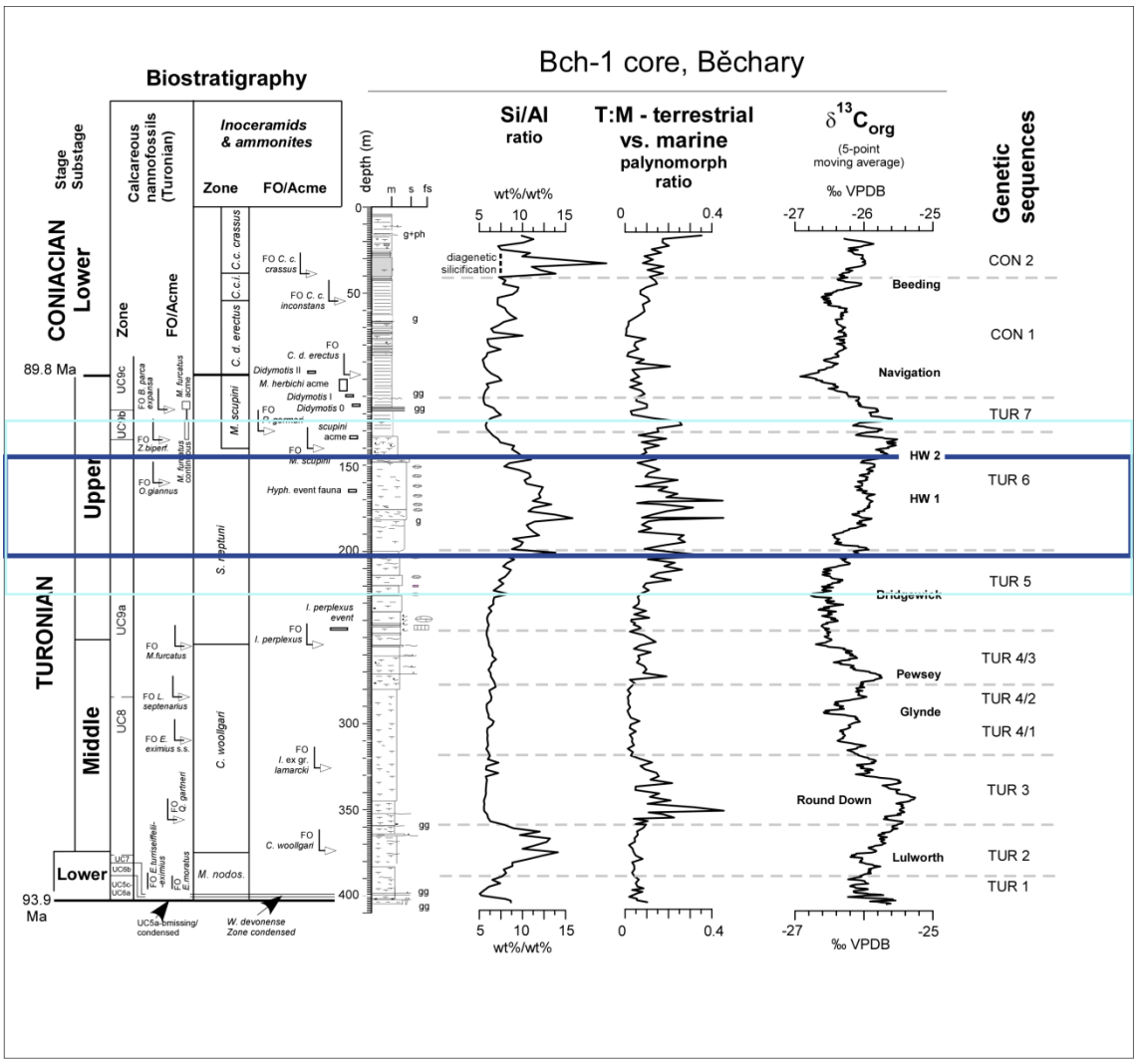

Fig 2.3-1

Figure adjusted after Uličný et al. submitted. There is a pronounced interval of higher Si/Al values accompanied by distinct variability in the T:M ratio. That and the occurrence of several very pronounced carbonatic beds or nodules, was one of the reasons for selecting this interval for further study.

2.3.1.1 Tectonic history, Paleogeography and Stratigraphy of the studied interval

The stratigraphic interval chosen for this study falls within the Upper Turonian as defined by the first occurrence of *Inoceramus perplexus* (*Čech, 2011*). The uppermost part of the offshore Jizera Formation and lower part of the Teplice Formation, as defined in the south-west, will be inspected, particularly their boundary and lower part of Teplice Fm. The interval is equivalent to the boundary between TUR 5 and TUR 6 and the lower parts of the TUR 6 sequence (*Laurin & Uličný, 2004*).

The Jizera Formation in BCB was defined as characterized by a more extensive sandy sedimentation and by marlstone - marly siltstone – sandstone cycles; in the central part of the basin the unit consists of marlstone locally with intercalations clayey

biomicritic limestones (*Čech et al., 1980*). These two deposits were informally divided into enarshore and offshore facies of the Jizera Formation (*Laurin & Uličný, 2004*).

The Teplice Formation lower boundary is sharp and erosive in the south-west and characterised by a higher content of glauconite, phosphatic nodules and coprolites (*Čech et al., 1996)* and other parts of the basin a glauconitic horizon is sometimes developed (*Čech et al., 1980*). The whole interval is characteristic by being the most pelitic in the BCB succession (*Valečka, 1979*) and is represented by a sequence of calcareous claystones to marlstones in the distal areas (*Čech et al., 1980*). Teplice Formation sandstones to the NNW margin of BCB are finer grained, partly calcareous with silty and clayey admixture (*Valečka, 1979*). Rohatce Member, occurring on top of the Teplice Formation succession, is time transgressive (*Malkovský, 1974*).

Both genetic sequences TUR 5 and TUR 6 fall within phase II of tectonosedimentary history (*Uličný et al., 2003*). Aggradation sequences dominated the succession in both intervals, but while there is a relatively slow intrabasinal faulting during TUR 5, a marked acceleration in the subsidence north of the Labe-Železné hory fault zone occurred during TUR 6 (*Uličný et al., 2009*).

2.3.1.2 Distinct features of the study interval

The south-western part of the basin has been intensively studied (*e.g. Krutský et al., 1975, Čech et al., 1996; Laurin & Uličný, 2004; Wiese et al., 2004)*

The secular onset of the carbonate-dominated conditions at the base of Teplice Formation was originally interpreted as a major transgression surface (*Malkovský, 1974; Valečka & Skoček 1990*). This in not necessarily in contrast to the observed influx of boreal fauna assemblages(*Wiese et al., 2004*) interpreted as a result of improved water circulation and an acceleration in the water-mass exchange with the pelagic carbonate factory of NW Europe (*Laurin & Uličný, 2004*). However, the glauconitic and phosphate horizons in Úpohlavy (*Čech et al., 1996)* do not necessarily have to be a sign of deepening. Locally reduced sedimentation rates of this interval (*Malkovský, 1987*) this could be caused by other mechanisms such as reworking by seafloor currents (*Nichols, 2009*). Moreover, the glauconitic horizons, that should have documented the transgression elsewhere, do not occur synchronously and are missing around Hradec Králové (*Herčík et al., 1999*). Laurin and Uličný (*2004*) revealed that the onset of carbonate deposition was coincided with a major change in differential subsidence/uplift pattern of the BCB and might have facilitated the mentioned change in circulation.

The rhythmic variation in carbonate content of the distal facies has been described already by Valečka and Skoček (*1990*) but further study was proposed in order to draw a conclusion about their origin. The cyclicity was further investigated; hemipelagic couplets and two orders of bundles were recognised and attributed to the climatic oscillations driven by the Milankovitch orbital cycles, particularly the long eccentricity cycle but also possibly the precession (*Laurin & Uličný, 2004*). The variations in lithology were explained by siliciclastic dilution, possibly coupled with changes in carbonate production (*Laurin & Vodrážka, 2010*). The changes in siliciclastic flux were so far attributed to transgressive-regressive movements of the shoreline.

3 Methodology

3.1 Core description

The fundamental technique of a lithologic description was performed on the selected 57 metres of core; this included the assessment of the colour, grain size and structures. Since the lithology is dominantly fine-grained, the number of observations has been limited mainly to that of colour and coherency (*Tucker, 2001*); however, several useful details were obtained.

Particular attention was given to the variability of bioturbation. Relative abundance and grain size characteristics of the coarser fraction were documented together with synsedimentary features. The grain size estimation was determined using a hand lens and a grain size chart. Areas of increased large bioclast accumulation were also pinpointed.

3.2 Sediment colour record and image analysis

Based on the fact that the major lithologic differences in Bch-1 (145-202) are accompanied by a systematic shift in colour between dark gray to light gray/white we decided to quantify this property for further investigation. Since the sediment colour is dependent on the sediment composition (*Tucker, 2001*), it is meaningful to study this property when tracing the origin of the lithologic variations.

The colour parameters are known to be a good tool for frequency assessment of lithologic variation (*Lamoureux & Bollmann, 2004*) and this fact has been used by many scientists studying the variability of sediment especially varves, loess and paleosols (*Porter, 2000*) but also marine cores (*Nederbragt & Thurow, 2004*) as well as Cretaceous pelagic marls (*Hinnov, 2000; Grippo et al., 2004*) and limestone (*Meyers & Sageman, 2007*). This type of dataset is especially useful due to its high resolution which makes it one of the best methods in respect to the data collection densities (*Hinnov, 2000*). A major drawback is the fact that the dataset on its own does not bear much information on the origin of the colour variation (*Lamoureux & Bollmann, 2004)*;

Although these limitations have to be taken into account, this method allows for the inexpensive acquisition of the millimetre scale resolution data and keeping to some basic rules (*Lamoureux & Bollmann, 2004*) it fits into the standardised requirement of repeatable experimentation.

A lot of preparation time was spent on perfecting the image acquisition process, since the poor quality of the image could create significant problems during subsequent analysis (*Francus et al., 2004*), and so based on many tests and literature recommendations, the following setup was arrived in **fig. 3.2-1.**

Fig 3.2-1
An Illustration photo of the setup arrangement with tripod and Fomei Basic lighting, all measures in cm. The core was photographed in a complete dark room where only source of light were the cable connected external camera flash lights to eliminate any interaction of the changing daylight illumination during the process of photo acquisition. Camera was placed on a tripod to ascertain unchanging distance between the camera and core. The external shutter release was used to diminish the possible mechanical disturbances.

The digital camera used was a reflex Nikon D3100 with a AF-S NIKKOR lens with 35 cm focal length (the traditional 52), 1:1, with professional external lighting system Fomei Basic 200, which enables the use of the diffuse-light umbrellas to provide better lighting and reduce glare and shadows. The settings on the camera were kept fixed on the fully manual of 1/100 seconds exposure time, ISO 100 and F-stop f/13. The image acquired was saved in jpg file format, which compresses four pixels into one.

The core was photographed in roughly 30 cm segments with a high percentage of overlap between photographs, see **attached CD** for the resulting 400 photos. Each picture is accompanied by a tape measure for scale, information on depth position, small grayscale and colour chart BST13 for colour calibration. The gray card GC18 was used as a reference for light intensity variation.

The photographs were consequently used for image analysis and processed using several programs (see section on software below) to create a continuous grayscale log. The extraction of the depth series of grayscale value from photographs provides the means to characterising the stratigraphy of the marine sequence in fine detail (*Ortiz & O'Connell, 2004*), and the general practice is to correlate this data to physical and chemical properties in the sediment.

Although it has been suggested that the stratigraphic interpretations of simple grayscale colour data can be affected by a significant error related to the chromacity (*Koptíková et al., 2010*), in our case this has been partly mitigated by the fact that the studied succession by itself is rather monochromatic.

The grayscale values are displayed as an optical density log with values ranging from 0 to 255 (*Ortiz & O'Connell, 2004*) based on an 8-bit integer. The numerical value itself however, is not of major importance; the main output being the resultant log as a faithful representative of the relative difference in gray shades between the lithologies.

The grayscale data values are directly linked to the colour of the sediment, which in turn is dependent on mineral composition and so it can be postulated that the log does reflect compositional changes. These changes can reflect both the depositional and post-depositional history of a succession but when the dominant colour carriers are identified it can lead to meaningful sedimentological interpretations.

3.3 Micropetrology

Inspecting thin sections under a petrographic microscope brings invaluable information about mineral content and the detailed structural relationships between constituents of the examined rock; providing material for further environmental interpretation.

It allows for a direct measurement of the grain size of fine-grained clasts and a volumetric estimation of other components, both of which are important for various sediment classification schemes. The differentiation in grain size fractions and the identification of some smaller bioclasts would otherwise be very problematic.

While data on grain size, roundness and sorting provides hints to the length of transport from the source area and/or processes involved during deposition, the synsedimentary features, when present, provide more specific clues. Moreover, the post-depositional history record is preserved within the micro-scale arrangement (*Scholle, 1979*), holding crucial information for alterations during early and later diagenesis.

The eighteen samples for inspection were selected based on previous lithologic investigations of the core to represent some of the most interesting phenomena and to investigate places showing pronounced colour variations. Six more thin sections were obtained from an earlier Bch-1 investigation.

The Nikon microscope Eclipse 80i and Nikon camera (GFÚ AV ČR) and Nikon Eclipse E600 with Canon camera (PřF UK) with the magnification of 2, 5, 10 and 20 were used.

The roundness, angularity and relative volume percentage of individual components was assessed using comparison charts such as those published in Adams et al. (*1984*). Size characteristics of grains were based on 20 random grain samples for quartz, glauconite and foraminifers with separate search for the minimum and maximum values of quartz grains. For muscovite usually about five grains were measured along the longest axis, other measurements are based on one sample evaluated to be representative of the median of other specimens.

3.4 Geochemistry

Geochemistry is another method which offers a glimpse into sediment composition; through the relative mass percentage of the various oxides a tentative estimate of the different mineral fractions can be established. This is especially useful since in fine grained sediments, such as mudstones and marlstones, the composition is rarely revealed with a mere visual inspection.

Geochemical proxies for different sedimentary fractions can be established; for example in calcareous samples, such as ours, it is possible to consider most of the CaO as calcite forming. This value is in a shallow basin proportional to the biogenic flux (*Sageman & Lyons, 2004*), although the origin of calcite should be investigated. Different depositional processes would be assigned to an accumulation of coarse-grained shell fragments or fine carbonate mud, not to mention the possibility of post-depositional diagenetic effects. For the separation of these, however, other methods are needed.

Another element concentration data is also in use. Elements such as Al, Ti and Zr are predominantly transported to the ocean from external sources; ultimately these elements are of a continental origin (*Zabel et al., 1999*). For example, aluminium is considered the main conservative proxy for clay minerals (*Sageman & Lyons, 2004*) and titanium resides principally in heavy minerals such as ilmenite, rutile, anatase or sphene, and zirconium is found in zircon (*Jarvis et al., 2001*).

Silica is considered a proxy to detrital quartz silt in hemipelagic lithologies (*Sageman & Lyons, 2004*) even though silica occurs in a much wider range of sediment constituents including biogenic opal, glauconite and also in clay minerals to some extent (*Jarvis et al., 2001*).

The basic idea is that of assigning a particular element to be a proxy for a certain grain size fraction and considering its concentration changes to be proportional to this

fraction's presence. The element concentration data can suffer from the inherent limitations of reciprocal dilution (*Sageman & Lyons, 2004*) and measured values can react dramatically to the changes in the sedimentation rate. This is a reason why the element ratios were introduced, as they serve to normalize components in major dilutants and thus allow contributions to a flux variability to be isolated (*Sageman & Lyons, 2004*).

The silica and trace element to aluminium ratios have been used for interpreting the transgressive-regressive history (*Jarvis et al., 2001*) and even to distinguish orbitally driven trade wind variations (*Zabel et al., 1999*). However, any deliberations on element ratio variability is derived from some mechanisms allowing for the mixing of the assigned grain size fractions (*Laurin, in prep.*) and the correct interpretation of element proxies depends on distinguishing the element sources and transport modes (*Sageman & Lyons, 2004*).

The chemical composition was measured by a handheld x-ray fluorescence spectrometer Niton XL3t GOLDD from the Thermo Fisher Scientific with 50 kV roentgen lamp; the Test All Geo and Mining settings were used. Thirteen samples were taken from strategically selected locations, in order to cover the variability over some of the small scale lithology variations as well as capturing variations over the whole TUR5/TUR6 interval which would allow for comparison with already existing geochemical datasets and other locations. Measurements were performed on a powdered specimen of 6 g.

For information on calibration see **appendix 2**.

3.5 Magnetic susceptibility

Magnetic susceptibility (MS) has proven to be a powerful tool in the study of sedimentary record (*e.g. Porter, 2000; Koptíková et al., 2010, Bábek et al., 2011a)*. MS is a magnetic property of rocks showing their ability to be magnetized by the external magnetic field (*Dunlop & Özdemir, 1997*). It is defined as follows:

$$M = kH$$

Where M is induced magnetization in A/m, H is intensity of the magnetizing field also in A/m and k is magnetic dimensionless MS. The carriers of MS are minerals present in the sample; therefore, the measured value reflects mineral composition. Moreover, it is directly proportional to the concentration of these minerals (*Hrouda & Kahan, 1991*).

All minerals can be divided into three fundamental categories based on their magnetic structure; these are diamagnetic, paramagnetic and ferromagnetic minerals (*Dunlop & Özdemir, 1997*). A brief summary and classification of minerals common in marine sedimentary rocks follows.

Diamagnetic minerals are typical by their generally low and negative MS independent of the magnetising field and their presence reduces the overall MS of the sample. Quartz and calcite are the most common representatives in marine limestone and shales (*Ellwood et al., 2000*); their values are $-15.4 \cdot 10^{-6}$ and $-12.9 \cdot 10^{-6}$ SI respectively. Feldspars, aragonite and opal do fall into this category as well (*Hrouda et al., 2009*).

Paramagnetic minerals are characterised by positive MS values, generally an order or two higher than that of the diamagnetic minerals; their MS value is also independent of the magnetising field. For a synopsis of some paramagnetic minerals and their values see **Tab.1**; Pyrite, glauconite and clay minerals also belong in this group (*Stage, 2001; Lurcock & Wilson, in press*).

Ferromagnetic minerals often bear a very high and positive MS, which is a complex function of the measuring field; these minerals also have the ability to retain remanent magnetization (*Dunlop & Özdemir, 1997*). Magnetite is one of the most common ferromagnetic minerals in marine sedimentary rocks (*Chang' & Kirschwing, 1989; Kößler et al, 2001; Stage, 2001*). Magnetite in the rocks can be detritic, early diagenetic, for example, produced by microbacterial activity, and possibly also in the form of magnetofossil (*Chang' & Kirschwing, 1989*); size and other magnetic properties of the magnetite grains help to distinguish between these types. The MS values of magnetite are 3-4 SI (*Hrouda et al., 2009*).

It has been pointed out that MS by itself has a limited paleoclimatic interpretation value, suggesting a need to be combined with other climatic indicators for the studied environment (*Mayer & Appel, 1999*). Numerous studies of fossiliferous deep-sea sediment cores reflecting different marine environments, have demonstrated a pronounced climate control and coincidence with earth-orbital parameters (*Kößler et al., 2001*); these observations as well as the cyclic nature of some of the MS records have led some scientists to use MS to help to identify the Milankovitch cyclicity (*Mayer & Appel, 1999; Kößler et al., 2001*).

However, it has to be noted that MS can easily reflect a water level change, independent of climatic factors, as well as diagenetic processes of siderite or magnetite enrichment. To help us differentiate between the various scenarios, a careful observation of the mineral composition from the studied sediment, as well as the origin of mineralization, is vital. The regularity or the lack of it within the MS variations also bears additional information. In any case MS is a powerful tool in interpretating the nature and causes of cycles preserved in the marine realm (*Kößler et al., 2001*).

Tab.1

This table shows values of paramagnetic minerals common in sedimentary rocks and their bulk susceptibility, after Hrouda et al., 2009. Note that the values of paramagnetic minerals are not a single value as in the case of lower-valued diamagnetics (see text above); this variation is dependent on the chemical composition of those minerals such as the Mg/Fe ratio.

Mineral	Susceptibility $[10^{-6}]$ SI	Mineral	Susceptibility $[10^{-6}]$ SI
Muscovite	36 to 711	Tourmaline	39 to 1,520
Biotite	873 to 3,040	Epidote	1,010
Phlogopite	176 to 281	Zircon	-15 to 386
Lepidolite	136 to 1,560	Garnet	553 to 6,230
Siderite	2,770 to 3,170	Rutile	107
		Ilmenite	8,042
Orthopyroxene	3,670		
Clinopyroxene	613 to 25	Pyrite	-6.3 to 63
Hornblende	746 to 1,368		

The main advantage of this method is the relative speed with which a large scope of data can be obtained; MS measurements are also easily applicable, non-destructive and inexpensive. A log of continuous and extended records needed for useful paleoclimatic reconstructions can be obtained (*Mayer & Appel, 1999*).

The Bch-1 core was investigated for MS, using Kappameter KT-10 (manufactured by Georadis Ltd., Brno, Czech Republic), with improved sensitivity of 1×10^{-6} SI (according to the statement of the manufacturer); this instrument takes the measurement in a magnetic field lower than 1 A/m. The measurements were made on the core side and corresponding corrections for the core diameter were made, which is an option built into the instrument. Controlled by the size of measuring coil, the readings are an average of five-to-six centimetre segments of the rock.

21 control samples were taken for a bulk magnetic susceptibility measurement on MFK-1 Multi-Function Kappabridge (Agico Ltd., Brno, Czech Republic) from key locations based on lithology and the Kappameter measured MS. These measurements served as an independent check on the MS data values, with the advantage of higher sensitivity of 4×10^{-8} SI and outstanding measurement precision with a maximum of 1-3 percent relative error (*Pokorný et al., 2011*). The kappameter measurements were calibrated to the kappabridge results, see **appendix 3**. The driving field of 200 A/m and operating frequencies of 976, 3904 and 15616 Hz were used.

An investigation of the variation of bulk MS with temperature is a powerful tool for the identification of MS bearing minerals in the rock (*Hrouda, 1994*). Diamagnetic materials show no variation of MS with temperature. Any variations of MS of the paramagnetic minerals is represented by the hyperbola, in ferromagnetic minerals, on the other hand, there are acute drops in susceptibility at certain temperatures when magnetic crystalline states are changed (*Hrouda et al., 2009*). This test was performed on powdered specimens using the MFK1-FA in cooperation with non-magnetic CS-L Cryostat Apparatus in temperatures intervals between the temperature of liquid nitrogen (-196 ^0C) and zero (*Pokorný et al., 2011*). This method is designed to reveal the prevailing component bearing MS of the rock. The principle of this method for MS resolution into paramagnetic and ferromagnetic components is illustrated in **Fig. 3.5-1**, the method being executable by the program CUREVAL developed in AGICO Ltd. Brno.

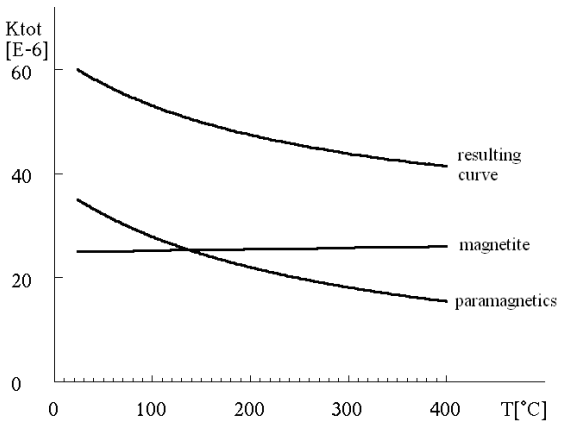

Fig 3.5-1
The simplest model of MS vs. temperature curve of a rock containing paramagnetic minerals and one ferromagnetic mineral, which considers the ferromagnetic susceptibility to be constant.

$$k = p_p C/T + p_f k_f$$

Where k is rock susceptibility k_f *is ferromagnetic susceptibility within resolution interval,* p_p *and* p_f *are percentages of paramagnetic and ferromagnetic fractions, respectively, C is paramagnetic constant, and T is absolute temperature. Diamagnetic contribution is often negligible in value*

The calculation of the Maximum Theoretical Paramagnetic Susceptibility (MTPS) was performed; this concept, introduced by Aydin et al. in 2007 (*Hrouda, 2010*), is based on a theoretical calculation of the maximum paramagnetic susceptibility from the

chemically determined contents of Fe and Mn ions. The relationship between bulk paramagnetic susceptibility and the contents of Fe and Mn can be described as follows (*Hrouda, 2010*)

$$K_{MPTS} = d\left[2.696c_1\left(Fe^{2+}\right)+3.229c_2\left(Fe^{3+}\right)+3.282c_3\left(Mn^{2+}\right)\right]10^{-8}$$

where d is the rock density in $kg \cdot m^{-3}$ and c one to three are oxide weight percent concentrations of bivalent iron, trivalent iron and manganese, respectively.

3.6 Spectral analysis (SA)

This method was used in order to characterise the cyclicity within the core record. Except for very simple or especially characteristic data sets, it is unlikely to reveal regular cyclicity by visual inspection alone (*Weedon, 2003*). The dataset used for SA investigation, such as colour densitometry or MS, is called time-series. The time-series analysis plays a central role in cyclostratigraphy.

Time-series analysis is suited for the study of stratigraphic data because the succession of sedimentary rocks basically records the passing of geologic time; ideally, stratigraphic thickness can be converted directly to the length of time (*Mayer & Appel, 1999*) as long as an age model using well-dated layers at the top and bottom of the succession is established (*Kößler et al., 2001*).

Sine and cosine waves are convenient for mathematically describing oscillation (*Weedon, 2003*) a concept upon which most SA methods is based. Statistical significance of a signal can be determined by testing against a "noise" model series (*Hinnov, 2000*). The resultant power spectrum shows squared amplitudes and wavelengths (or periods) of regular components in the time series (*Weedon, 2003*) see **fig. 3.6-1**.

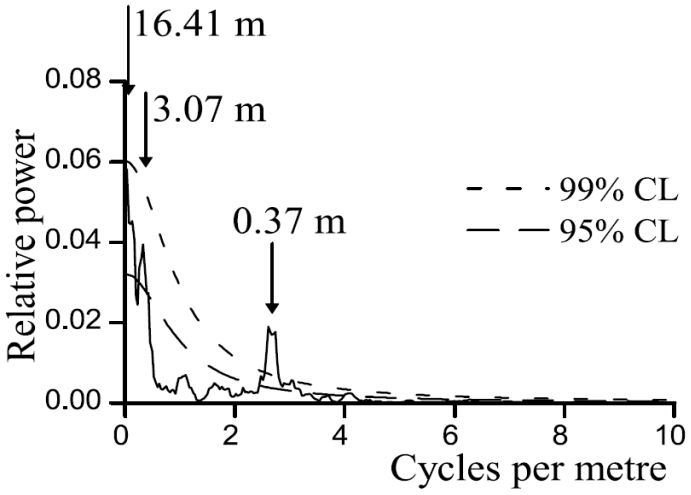

Fig 3.6-1
After Weedon kniha. By convention the horizontal axis of a power spectrum is plotted as a frequency with higher frequencies appearing on the right. The height of the peak on y axes answers to the amplitude of the oscillation. The dashed lines signify the position of confidence level with which the signal reaching above the line is significant. Data below the line are considered noise.

Several geological processes can distort the original environmental signal; most common among them are irregularities in the sediment accumulation, bioturbation and diagenesis. These processes destroy rather than create regularity and reduce the chances of distinguishing peaks from the background in the power spectrum, therefore if a regular cyclicity is detected, it can be concluded that a regular cycle in time was the cause (*Weedon, 2003*).

Different spectral techniques employ different methods in order to obtain the best spectral estimation (*Weedon, 2003*).

The potential presence of periodic signal in the study interval was examined with the Multitaper Method (MTM) spectral estimate (*Thomson, 1982; modified after Mann & Lees, 1996*) using the Analyseries software, v. 2.0.4.2 (*Paillard et al., 1996*) and kSpectra Toolkit (SpectraWorks). Vertical changes in the depth-domain frequencies of the hypothesized orbital components were traced using the Evolutive Harmonic Analysis (*Meyers et al., 2001*), which is a moving-window modification of the original MTM with an independent significance test (F-test).

3.7 Other software

Some programs used for processing and viewing information, have already been mentioned. In this section a list and a brief description of these follows.

ImageJ is a public domain Java image processing and analysis program with available spatial calibrations and the possibility to calculate pixel value statistics. It was used to quantify the colour information from core photographs. Working with the photographs saved in Tiff format to avoid further data loss, each photo was first converted into a

grayscale, using the internal program algorithm, then scaled down to the number of pixels corresponding to the millimetres of length based on the tape measure reading. When this was achieved a window of 20 pixels was placed over the crest of the core from which the column average pixel intensity value was calculated, see **fig. 3.7-1** for the determination process of the 20 pixel value. The resultant output was a text document (Tab.delimited) containing an array of assigned numerical grayscale values expressing the optical density of the sample.

A program, courtesy of Prof. Hrouda, was used for connecting the colour information into a continuous depth series. This program allows for a quick manipulation with uploaded text (space delimited) with optional x-y shifts of the uploaded curves based on their shared overlap and results in creation of a longer master text document. When all the individual consecutive tables are uploaded, the master document is represented by a single long depth series stretching over the length of the core where each entry represents a grayscale value.

Canvas 14 was used for adjusting the illustration photographs and drawing illustrations. The traditional data viewing and processing programs such as MS Excel and Grapher were also used.

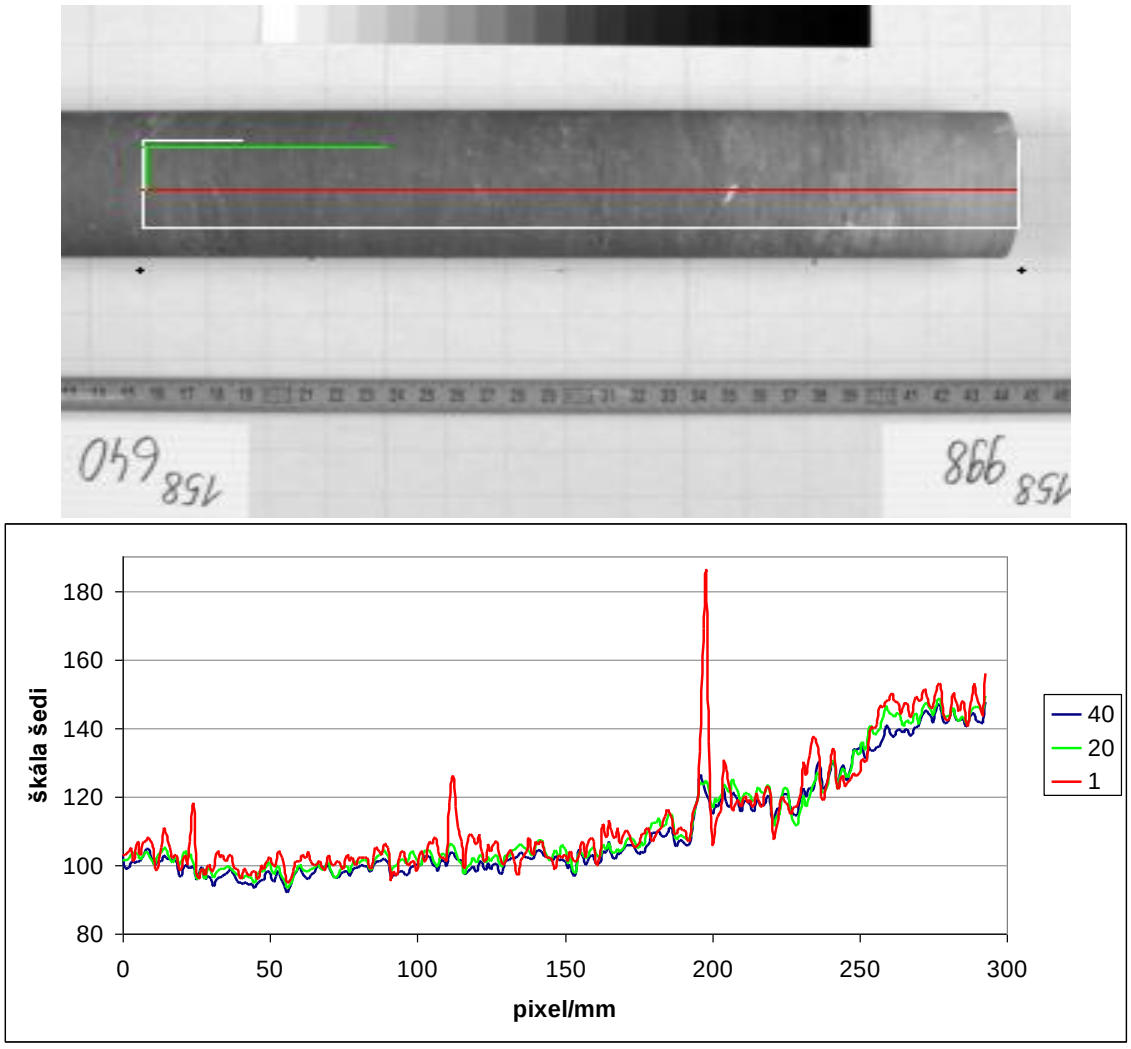

Fig 3.7-1

Showing test situation where the rectangle of the width of 1, 20 and 40 px was used. While one pixel line shows pronounced fluctuation the other two are more averaged – balanced highlighting the long term trend, that is why horizontal change in colour is best dealt with by profiling images using multi-pixel line widths (Porter, 2000) the 36 px line is already showing an effect of including the shaded edge pixel rows. The choice of width of the stratigraphic line or a bar is partly a matter of preference and can be varied depending on the type of the sediment or quality of the camera that was used (Francus et al., 2004) The length and width of this window was carefully picked to represent the widest possible rectangle without including any of the photo-inherent adverse effects such as shadows and shape deformation.

4 Results

4.1 Lithology description

In this chapter, data from the visual inspection of the Bch-1 core lithology at depths of 202 to 145 m are discussed, with the intention to present the data, as well as the succession in which data were acquired. Firstly, lithotypes were defined based on the core description and then samples for micropetrographic inspection were selected to further investigate the observed features. The interpretation presented at the end of the chapter is based on a synthesis of macro- and micro-petrography.

4.1.1 Core description

The succession is mostly muddy in grain size with some carbonate content; a low amount of silt to fine grain sand grains however can be identified in most samples.

While there were many coarse bioclasts identified in the core, most of them were too small or broken for identification. However, some inoceramus shell fragments were possible to identify because of their prismatic calcite shells. Phosphatic clasts were identified at the depths of 149.7, 155 and 198.5 m.

4.1.1.1 Bioturbation

Bioturbation is common along the whole length of the studied interval and can be characterised by the intensity grade four to six as defined in MacEachern et al. (*2010*). These grades describe the variability between the common bioturbation with indistinct bedding boundaries and the complete bioturbation resulting in total biogenic homogenisation of the sediment. Evidence for the depositional mechanisms is therefore limited.

Among the most common intrastratal ichnofossils observed are *Anconichnus*, *Planolites*, *Thallassinoides*, *Asterosoma*, occasional *Roselia* and possibly also *Teichichnus*. Most of these would fit into the Ceruziana ichnofacies (*Pek & Mikuláš, 1996*). In several instances cross-cutting relationships can be observed, see **fig. 4.1-1,** and a notable difference between the compaction of trace fossils within and outside of the light lithology exists, see **fig. 4.1-1**.

All pictures are shown with the original sediment position (the younger stratigraphy is to the top of the picture) and the width of the frame is the width of the core - 6 cm for scale.

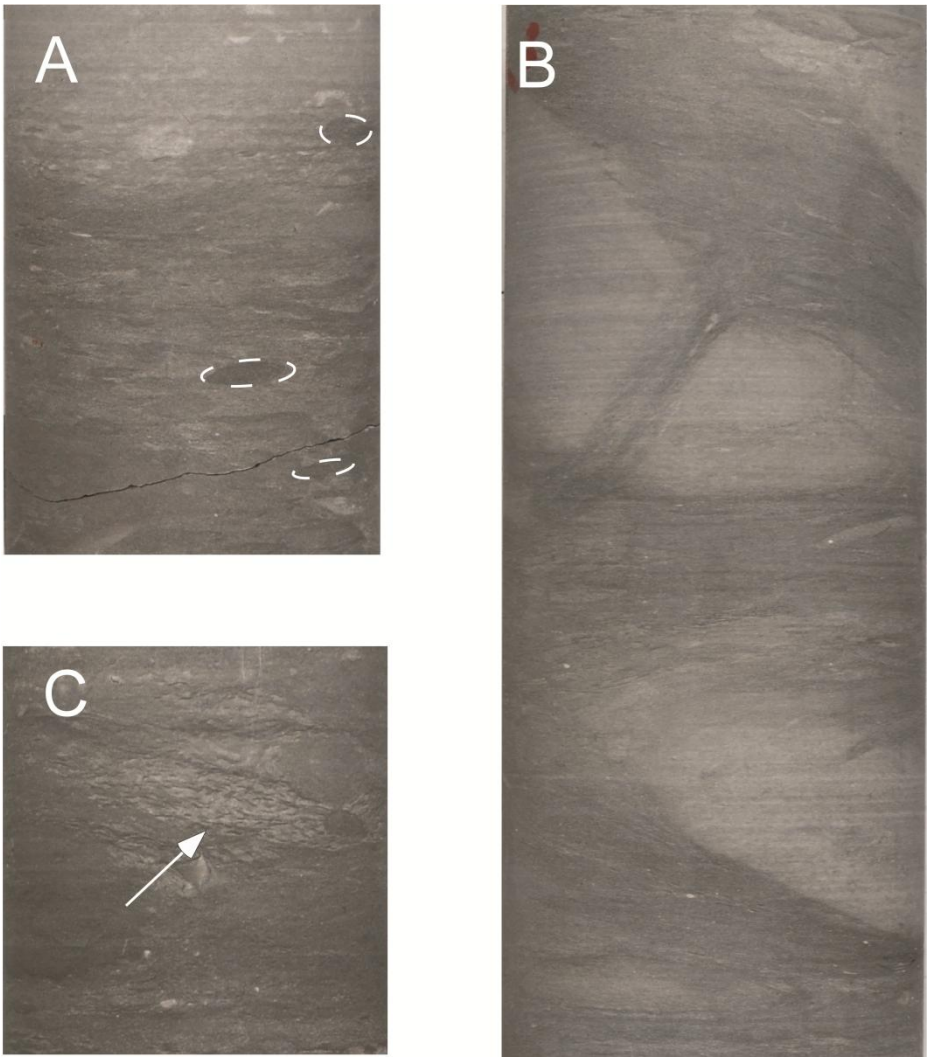

Fig 4.1-1
Showing some of the trace fossils occurring in the core. Thin blue colour line was used to highlight the less obvious features.
A) The figure shows an example of the Lithotype III bed (on top in this case tied to the occurrence of large Thallassinoides. Very interesting is the early diagenetic preservation of originally round cross-section of younger traces which goes progressively flattened towards the edge. Some differential compaction of sediment along the edge of the concretion represented by bent laminae is discernible in several samples
B) The figure below shows an example of the Lithotype III, in this case tied to the occurrence of large Thallassinoides. It is cross-cut by another trace which of a sign of a many times reworked sediment with developed tiering system.
C) Anconichnus is very common in the core.
Positions: 179.4 A, 183.3 B, 178.4 C

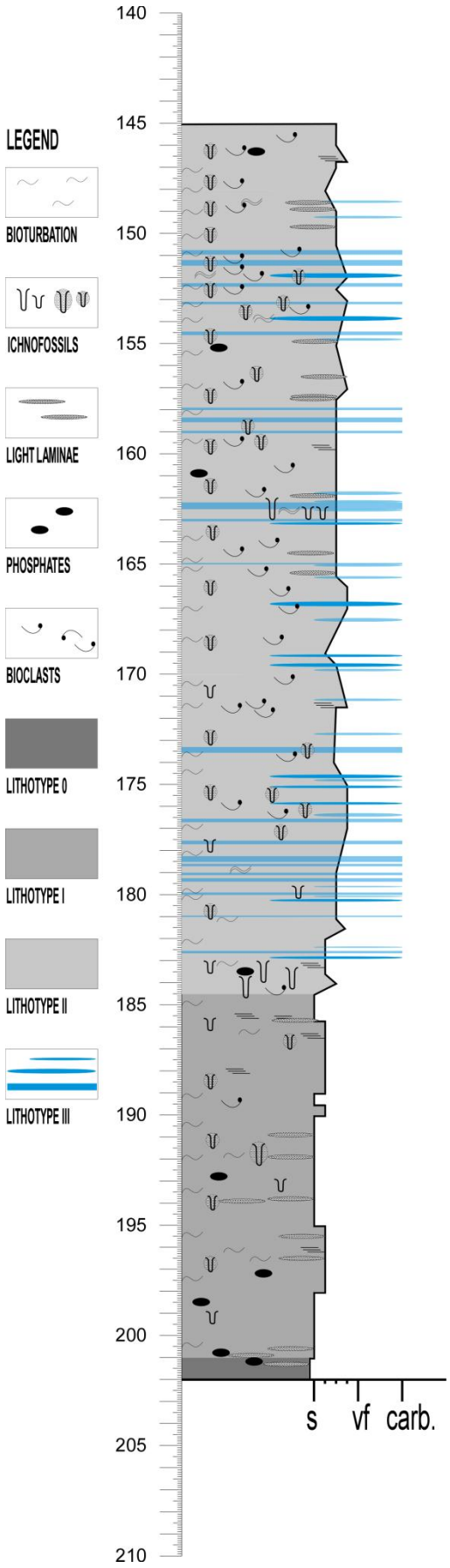

The colour and firmness did vary over the core. The older strata (184.5-202 m) are light to dark gray, the younger deposits show distinct rhythmic white-to-gray variations in colour. These facts led to an early division into four main lithofacies; two occur at the upper forty meters and two precede them, see **fig. 4.1-2** for the core log and description of the lithotypes.

4.1.1.2 Lithotype 0

Is light to dark gray brittle lithology at the bottom of the core (200-202 m), very similar to the lithotype I but with lower silt size fraction.

4.1.1.3 Lithotype I

At the depth of 184.5-200 m it is light to dark gray and dominated by a very fine carbonate and clay matrix with a relatively lower size of silt sized grains. The occasional remnants of original lamination are observable. A higher number of lighter, seemingly coarser, laminae were identified. The boundary between Lithotype I and lithotype II is gradual yet highlighted by the colour contrast.

Fig 4.1-2
Core log showing the core lithology. Depth is on vertical axis, grain size of the coarser admixture in mudstone on horizontal axis.
Left hand "regular" side on the diagram features long-term bioturbation and Anconichnus abundances, the right hand shows position of prominent traces, bioclasts and laminae.
The blue horizontal bars refer to carbonatic Lithotype III, where a distinction was made between continuous layer, layer showing some variation in thickness and nodules bearing same properties

4.1.1.4 Lithotype II

Lithology II and III – are both present between the depths of 145-184.5 m. The boundaries between the two are distinct but gradual, never displaying erosional features.

Lithotype II forms the darker interval of many cycles, it dominates the upper part of the core and is characterised by s light gray colour and variable silt admixture. A notable local grain size maxima occurs at 147.6 and 171.5 m, see **fig. 4.1-3**, and displays a somewhat abrupt change from a lower muddy layer into overlying more silty sediment.

Glauconite and bioclasts are relatively abundant, and in several locations coarse, from few mm to cm long, bioclastic shard accumulations occur, for example at the depths of 148.7, 159.6 or 172.5 but also elsewhere in the core. The bioturbation is high to complete; individual traces abundance varies however, with long-term minima between 145-150 m and 165-175 m.

4.1.1.5 Lithotype III

Lithotype III is typical with its comparably white colour and high firmness. Upon first inspection, it shows a higher carbonatic content and a small percentage of silty admixture. It forms thin, up to 30 cm wide, beds and concretions. No particular bioturbation pattern seems to be connected with this lithology, although some of the nodular representatives appear to be following an original burrow fill, see **fig. 4.1-2.**

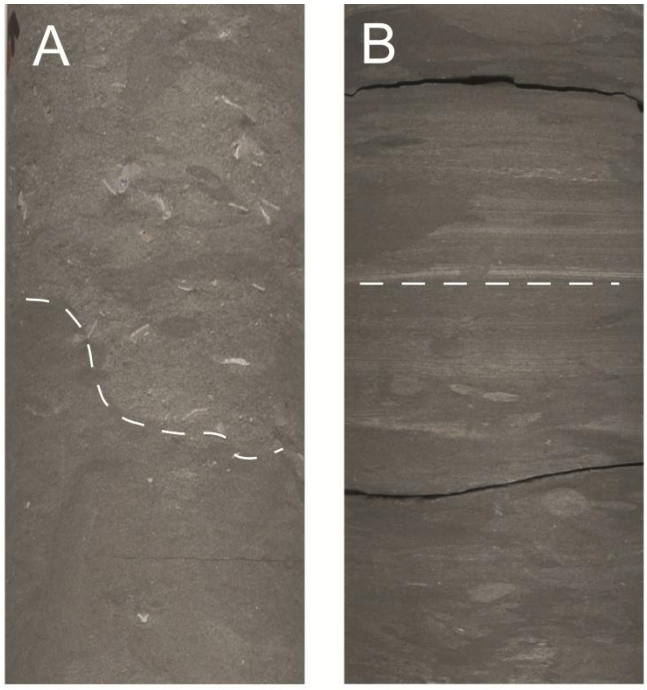

Fig 4.1-3
Two of the most distinct sedimentary structures observed on the core. First type is one of the two boundaries with coarser grained lithology overlying a muddier interval (A) and preserved lamination (B), especially around 184.5-185.5 Positions:147.5 A, 183.3 B.

4.1.2 Micropetrography

The systematic study of thin sections has yielded several observations with the majority of the compositional characteristics common to all of the inspected samples. The focus of the micropetrology investigation was centred on the rhythmic lithology variations between Lithotype II and III, fifteen out of the twenty four thin sections were chosen to reflect this fact. The remaining nine thin sections were focused on lamination, Lithotype III type concretions, with an inspection of the isolated coarser laminae and the difference between the Lithotype I and 0. See **Tab.2** for an overview.

All of the samples are typical in their prevalence of a fine grained matrix consisting of carbonate with some non-quantifiable clay admixtures. The clay admixture was visually confirmed by uniform extinctions of large matrix areas due to the preferential orientation of clay crystals.

Bioclast shards of echinoderms and both thick and thin-shelled molluscs are very common as well as fully preserved shells of various foraminifera, see **fig. 4.1-5** Although the amount of bioclast varies over the span of the core, between 1 to 10 % with most common value around 5 %, no detectable shift in their composition occurred. The less abundant bryozoans, urchin spines and ostracods were not detected in all thin sections but this should be viewed as a sign of their rarity since there are usually no more than three sightings per sample. Other, less certain finds, include sponge spicules within matrix and some phosphatic fragments.

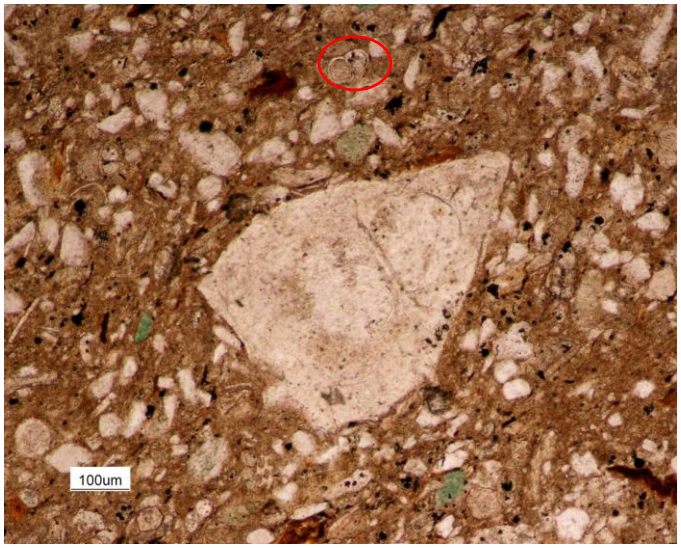

Fig 4.1-5
A big specimen of planktic foraminifera. It has a sparite infill the sediment around it shows signs of differential compaction. Note the much smaller specimen in top of the photo, which are a more common type and size occurring throughout the core. Their relatively small sizes, around 100 micrometers, do signify some sort of stress in the environment (Holcová personal communication)

Some percentage, of the coarser siliciclastic admixture was detected in all thin sections. This fraction is characterized by moderate to moderately-well sorted material with low sphericity grains and the angularity variability between sub-rounded and sub-angular. The average grain size generally falls into the upper part of the coarse silt limit with values around 55 micrometers, maximum clasts can however reach as much as fine sand sizes.

The main constituents are quartz grains; the quartz is mostly monocrystaline with uniform extinction, although varieties with very abundant inclusions or undulose extinctions do occur. Some unusual, very angular quartz grains with a very high eccentricity of obscured origin were observed. Occasional feldspars and abundant but fine-grained muscovite (with a long axis, usually around 110 micrometers) are the two other most common clastic grains. Partly altered dark amphibole grains were also identified. Both accessory minerals and blue-to-yellow tourmalines and heavy minerals such as rutile, titanite and zircon are common.

Invariably present are the grains of framboidal pyrite, see **fig. 4.1-6**, often near to or confided inside the skeletal remains of various organisms, namely foraminifers; green glauconite grains are also prominent. Various specimens of recrystallised calcite are present, mainly those replacing the micritic matrix. Rare dolomite rhomboids were observed and a small amount of silicification was also confirmed in many of the samples

A number of light-orange to dark-brown particles of various shapes occurs throughout the core, some seem more organic, some almost micaceous and others showing almost crystal shapes. Some fit into the Scholle *(1978)* description of plant fragments and their percentage varies from 1 to 10 percent. It is possible that some limonite or hematite has been misplaced into this group.

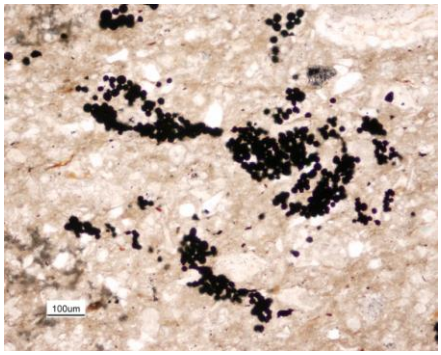

Fig 4.1-6
The spheroidal aggregates in the centre of the picture are called framboids (Schallreuter, 1984) and they are common in sedimentary rocks. They consist of pyrite, common opaque mineral with brassy colour in reflected light (Hejtman and Konta, 1959). Framboidal pyrite is considered an authigenic mineral and forms under reducing conditions, often close to organic matter.

Tab.2

This table shows selected data from the thin-section investigation. The colour code follows the Lithotype differentiation: dark grey -Lithotype 0, grey –Lithotype 1, white – Lithotype II, blue – Lithotype III. The column „description" states the original motive for selecting the sample.
A gradual trend in dark lithotypes towards more clastic lithologies in the middle of the interval, it can be noted in the „silt" column.
The amount of glauconite increases gradually from Lithotype 0 upwards, possibly signifying a slowdown of sedimentation rate.
Trends between the silt fraction percentage and size can also be observed, the higher the percentage, the bigger the mean clast size.
Big difference can be observed in the amount of matrix and silt fraction between adjacent Lithotype II and III samples as well as less pronounced indication that Lithotype III, is somewhat better sorted than adjacent Lithotype II samples.

Depth	Description	Matrix [%]	Bioclasts [%]	Silt [%]	Glauconite [%]	Opaque minerals [%]	ORG+ [%]	Mean silt size [μm]	Sorting
146.08	Lamination	72	5	15	2	3	2	33	
146.55	Lamination	70	7	13	3	5	2	-	Very good
155.31	Burrow-in	89	5	2	1	2	1	37	Very good /Good
	Burrow-out	84	3	8	< 1	3	1	41.5	Very good /Good
158.5	Bch-1	86	5	5	1	2	1	38	Very Good
163.12	Lithotype II	50	27	20	1.5	4		53	Good
163.18	Lithotype III	85	5	7	< 1	5		46	Very good /Good
163.32	Lithotype II	70	8	15	3	3	1	51.5	Good
167.02	Bch-1	60	10	23	1	4	1	53.5	Good
171.85	Lithotype II	64	7	20	1	5	3	44	Good /Mod.good
172.05	Lithotype III	84	5	6	1	3	2	46	Good
172.94	Lithotype II	66	5	20	2	5	2	55.5	Good
177.29	Lithotype II	65	5	20	2	5	3	52.5	Good
177.53	Lithotype III	90	3	3	1	2	1	44.5	Good
177.72	Lithotype II	66	6	21	2	4	1	56	Good
179.53	Bch-1	90	4	3	< 1	2	1	48.5	Very good /Good
181.35	Lithotype II	74	5	15	< 1	3	2	50	Good /Mod.good
182.57	Lithotype III	92	2	5	< 1	2	1	49.5	Good
185.41	Lamination	70	5	18	< 1	4	2	41	Very good /Good
185.52	Lamination-fine	60	10	21	1	4	3	48	Good /Mod.Good
	Lamination-coarse	81	5	7	< 1	4	2	36	Very good /Good
188.66	Burrow	78	2	15	1	2	2	42.5	Good
189.57	Lamination	89	3	5	< 1	2	1	43.5	Very good /Good
199.04	Bch-1	80	1	16	< 1	3	1	39	Very good /Good
205.02	Bch-1	85	1	10	< 1	3	1	43.5	Good
214.52	Bch-1	90	4	3	< 1	2	1	29	Very good /Good

4.1.2.1 Long-term trends

Tab.2 shows the results of the observations of all thin-sections highlighting some of the long-term trends as well as contrasting properties of Lithotype II and III samples.

Clearly visible is a gradual trend in the dark lithotypes to more clastic lithologies towards the middle of the interval with values changing from mostly below thirty two percent to mostly above this value.

Some dependence between the silt fraction percentage and size can also be observed, the higher the percentage, the bigger the mean clast size. This is also the case in the difference between Lithologies II and III which appear systematically variable with smaller grains in Lithotype III compared to the adjacent Lithotype II samples.

The amount of opaque minerals varies between two and five percent with a small drift towards lower values down core and the amount of glauconite exhibits a steady decrease from as high as three percent to below one.

4.1.2.2 Lithotype 0

The Lithotype 0 is notable mainly for its low concentration of silt size material and therefore high matrix proportion, with a maximum grain size of around 115 micrometers. The matrix is not recrystallised. Some accessories, such as tourmaline and zircon, were not confirmed but other than this fact the silt sized particles did not show any other marked change. The amount of glauconite is always below one percent with a distinctly smaller grain size than elsewhere of only thirty micrometers compared to most common fifty micrometers.

4.1.2.3 Lithotype I

Lithotype I is very similar to Lithotype 0 with a higher percentage of silt and a higher maximum grain size of around 150 micrometers. The majority of the matrix is mostly not recrystallised, although some large, almost poikilotopic crystals, rarely occur. The amount of glauconite is around one percent.

4.1.2.4 Lithotype II

Lithotype II is very similar to Lithotype 0 and I with the matrix not recrystallised and the amount of silt is higher. The maximum grain size commonly reaches up to 200

micrometers. The amount of glauconite and silt fraction is characteristic of the difference between Lithotype II and Lithotype I and 0.

4.1.2.5 Lithotype III.

The major and most apparent difference between the light and the dark lithologies is the different stages of carbonate matrix recrystallisation, see **fig. 4.1-7** Lithotype III is characterised with a widely recrystallised fine grained spar matrix, with sizes from 5 to 25 micrometers and rarely bigger. Lithotype III samples generally have a higher fraction of matrix per area, proportionally, to this relative amount, all other constituents diminish. The silty fraction decrease in abundance is the most obvious but the amount of pyrite; glauconite and organic matter are likewise affected.

There is some controversy as to whether white calcareous concretions are of the same origin as horizontally continuous light layers of Lithotype III. The microscopy observation is ambiguous, while the recrystallisation of the matrix to microsparite is the same in both cases; the accompanying difference of silt fraction was not confirmed in nodules. The sample of a thin section is not sufficient to draw any conclusive inferences.

4.1.2.6 Sedimentary structures

What appeared as a light coarse laminae in the core are places always accompanied by recrystallised sparite matrix, which in some cases is the only difference in the surrounding material, which is especially the case under the depth of 190 m.

In lower sections of the core, however, distinct coarse grained lamination is present especially between 184 and 185 m. These laminae do not display erosional base and, apart from containing more coarse grained bioclasts, do not show any difference in the general constitution of the silt fraction elsewhere.

Secondary textures vary between Lithotype III and the dark Lithotypes. The dark lithotypes display some stylolite-like features, see **fig. 4.1-8**, and reveal grain contact and compression features as well as a deformation of the more ductile mica grains. Quartz dissolution and silicification are more widespread in these types.

In Lithotype III some of the original bioclastic content seems to be recrystallised as well as the matrix leaving characteristic “ghost fossil” shapes in the sparite matrix.

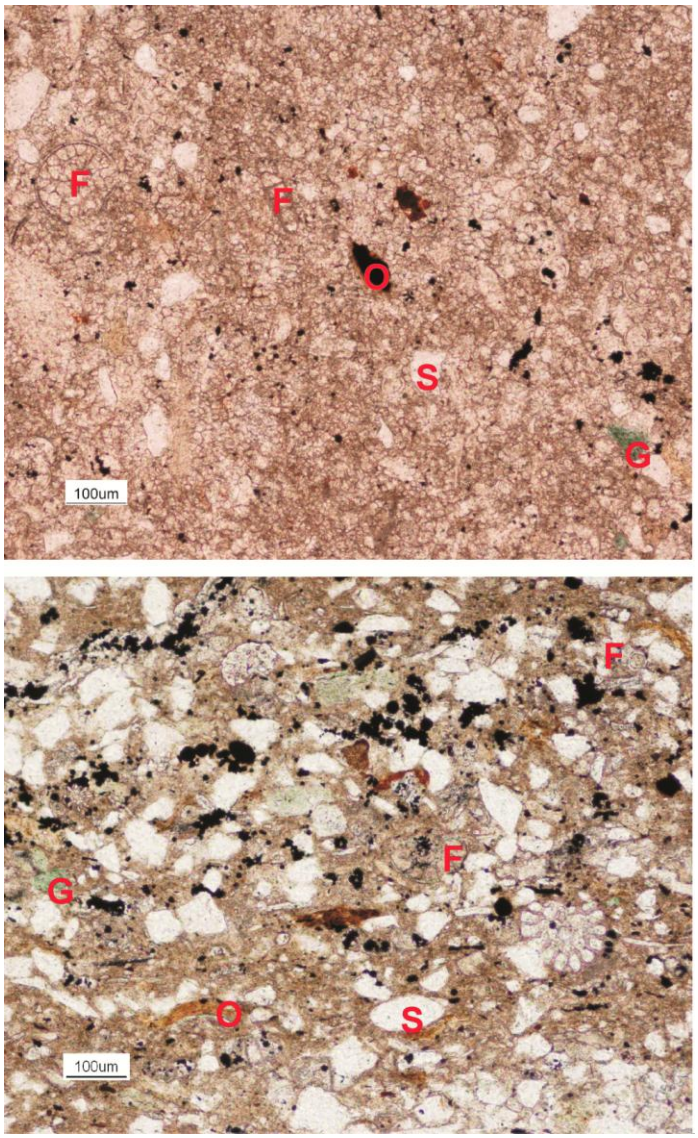

Fig 4.1-7
Comparison of lithotype III (at 163,18m) and lithotype II (at 172,72m) viewed in magnification ten. Notice the difference in matrix and silt grain abundances. S – silty quartz grains, G – glauconite, F – foraminifers, O – organic matter. The prominent fossil at the bottom picture was identified as an urchin spine cross-section.

Fig. 4.1-8
The dark hairline feature running through this photo is a sign of migration of fluids, most likely associated with compaction. The dark colour is caused by concentration of insoluble material such as clays and organic matter (Scholle, 1979) and such stylolites may provide a source of silica for the observed quartz cementation. These textures occur more commonly in Lithology II type samples.

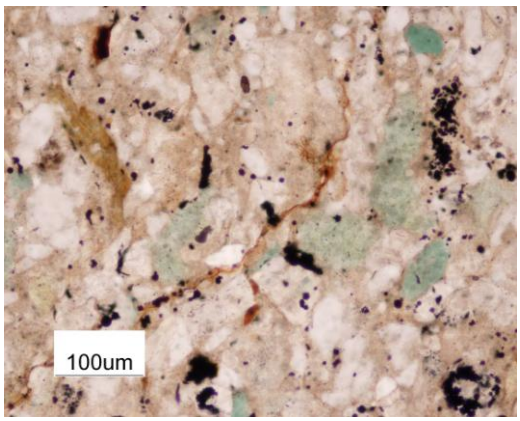

4.1.3 Interpretation

Impure limestones are problematic to classify, without chemical analysis the distinction between micritic mudrock or muddy micrite as defined by Mount (1985) cannot be resolved in our samples (*Flügel, 2010*). The classification of carbonate rocks has been used because the matrix appears to be mainly carbonatic and it is useful to distinguishing between the defined Lithotypes, although strictly taken the possibility of them having less than 50% of carbonate in the sample cannot be ruled out. The classification is based on data published by Scholle & Ulmer-Scholle (*2003*). The descriptive term silty should be used in all of the cases.

In Folk classification from 1952 and 1962 the thin sections are: Lithotype 0 biomicrite, Lithotype II and III coarse calcilutite: biomicrite and Lithotype III is very finely crystalline biosparite.

The revisited version of Dunham classification (1962) by Wright in 1992 is probably better suited for the differentiation between Lithotypes. Lithotype 0 is calcimudstone, Lithotype I is wackestone, Lithotype II would alternate between wackestone and condensed grainstone and Lithotype III is microsparstone.

4.1.3.1 Sedimentary constituents

The observed minerals and grain size fractions observed in the thin sections can be divided with respect to their origin into five groups.

Coarse siliciclastic minerals are extrabasinal in origin and their transport to distal regions of the basin depends on sediment supply and the accommodation space available for potential sediment accumulation close to the shore. The observed minerals belonging in this group are quartz, muscovite, hornblende, feldspar with accessory minerals like zircon, titanite, and rutile.

Clay mud is one of the matrix constituents; its amount fluctuates based on clay availability, which in turn may vary depending on transport paths and the energy of the environment which allows this fraction to settle (*Sageman and Lyons, 2004*). Unfortunately, little is known about the amount or type of clay minerals based on Micropetrography (*Adams et al., 1984*). Available data suggest that clay fraction is composed chiefly of kaolinite; illite and mixed illite-smectite structures are minor constituents, but increase in abundance with the onset of sequence TUR 6 (*Krutský et al., 1975; Laurin, unpublished data*)

Micrite is a biogenic component of the matrix and its quantity reflects the bioproductivity and/or energy of the environment.

Bioclasts are a diverse group, some of them were clastic and re-deposited as observed in the core description, yet some of them like the echinoderms fragments might have been deposited in situ and broken by overburdened pressure. Phosphates and some organic matter also belong in this group.

Diagenetic sparite and other minerals, such as pyrite, glauconite and dolomite, reflect changes that occurred in the sediment after deposition.

4.1.3.2 Observed Lithotypes

Lithotypes 0, I and II have many similarities but they do differ in the sedimentation rate and proportion of the siliciclastic component. Some variability in micrite to clay ratio in the muddy matrix can be expected based on their different colour attributes.

Lithotype III had a different diagenetic history to all the other lithologies, but it seems to highlight the original lithology difference characteristic of the smaller grain size, see **fig. 4.1-9**. The fine-grained sparite in Lithotype III has been identified as an early neomorphic microspar (*Scholle & Ulmer-Scholle, 2003*).

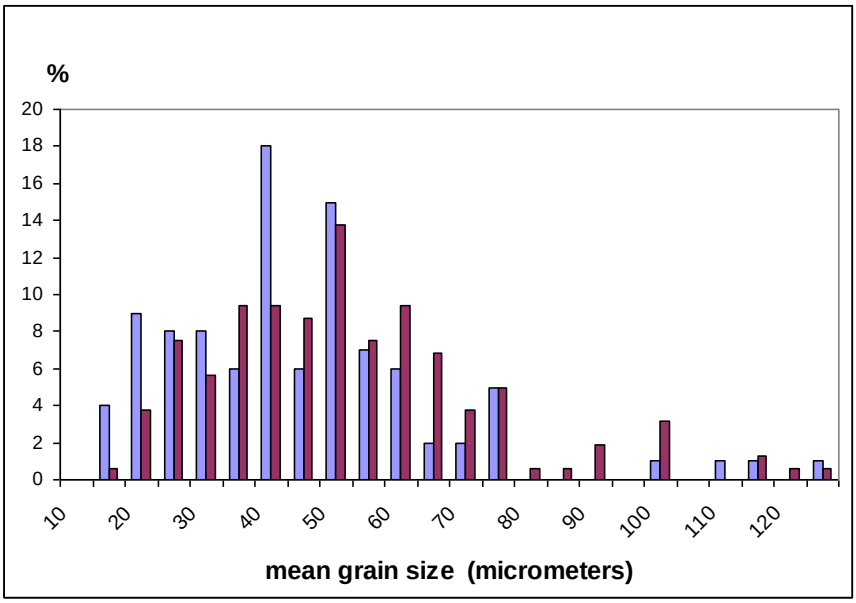

Fig. 4.1-9
Histogram of grain size distribution in percentages (vertical axis) for lithology III in blue colour, for lithology II in purple colour. Numeric values are based on internal microscope measure scale where 1 point equals 5 micrometers. Although not dramatic a certain offset towards lower values occurs for the Lithology III distribution.

4.1.3.3 General conclusions

Some generic information about the sedimentary environment can be drawn on, based on the observed phenomena; nevertheless it should always be kept in mind that the section has undergone some diagenetic modification and the system has been open to calcite and silica dissolution to some extent.

The transport of the coarser siliciclastic material was not very long based on the low roundness property of the grains as well as the fact that micas and hornblendes are still preserved (*Tucker, 2001*) and the source area of this fraction was most likely the same as for all of the observed Lithotypes as there was no marked difference in its composition. The mineral association and quartz silt characteristics shows mixed metamorphic, igneous and hydrothermal provenance.

The sedimentation rate was not constant throughout the interval with long-term slow down reflected by the accumulation of glauconite (*Tucker, 2001*).

The fact that the siliciclastic grain size distribution is not continuous but rather displays two non-overlapping peaks (silt and clay) is a sign of the two separate processes being in action. The non erosive nature of the lamination would point towards the sedimentation out of suspension.

The bottom waters must have been oxygenated for organisms to be able to survive (*Rotnicka, 2005*); their presence would contribute to the masking of the siliciclastic distribution signal. At the same time conditions within the sediment itself must have been locally reduced otherwise the early diagenetic pyrite could not be present (*Schallreuter, 1984*).

4.2 Collected data

This chapter gives a full overview of all datasets used for interpretation of the Bch-1 core lithology variability and their primary interpretation in terms of property carriers. In the first part all data logs used for secondary interpretation (cross-correlation and time-series analysis) are introduced, in the second part, a further description of these datasets, some additional measurements and the first interpretation in terms of property carriers are discussed.

4.2.1 Data logs

Data logs of both adopted and newly obtained data are presented here, with the characterisation of their variability. The adopted data is displayed over the interval

between 145 and 210 m for a better understanding of the character of environmental change leading into the studied interval.

4.2.1.1 Adopted Data

4.2.1.1.1 Carbonate content

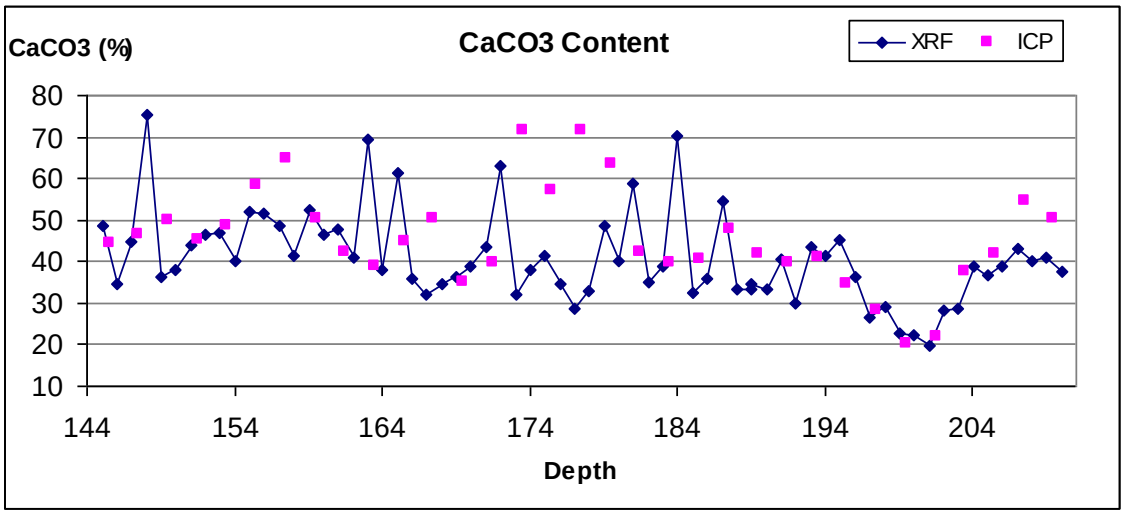

Fig 4.2 -1
XRF and ICP CaCO3 datasets at depths 145 to 210 m for description see text below. Note the pronounced minimum at around 202 m. XRF dataset is collected in one meter intervals and ICP dataset is collected in two meter intervals. The pronounced excursions of ICP data from the XRF trend are in fact real lithology variations.

The calcite equivalent molecular weight data from ICP and XRF measurements are shown in **fig. 4.2-1**, and the two datasets are comparable, see the next chapter. The data exhibits pronounced one point variability reaching over sixty percent carbonate from 184 m upwards. The global minimum was identified around 197-203 m and the maximum around 155 m. The local minima in a long-term trend are at 177 and 167 m, local maxima in a long-term trend are at 171, 180 m.

4.2.1.1.2 Element Ratios

ICP measurements were used for element ratio evaluation in the Bch-1 core due to the issues with the XRF dataset calibration. The plotted values are based on the percentage of Si, Ti and Al oxides and ppm of Zr amount in the sample.

On the **fig. 4.2-2** ratio between the aluminium normalised silica and the aluminium normalised zirconium is changing, while Zr/Al exhibits mostly increasing long-term tendency, and the silica trend has the highest values around 175 m and decreases both towards 145 and 205 m. Yet both display a global maximum of 181.5 and a minimum after 205, pronounced local minima and maxima between 147.5 and 151.5 m are also

displayed on both curves. Short-term variability appears to be mostly in phase, exceptions to this rule are at 155.5-161.5 m, 165.5-167.5 m, 175.5-179.5 m, 187.5-189.5 m, 195.5-197.5 m and 203.5 – 205.5 m.

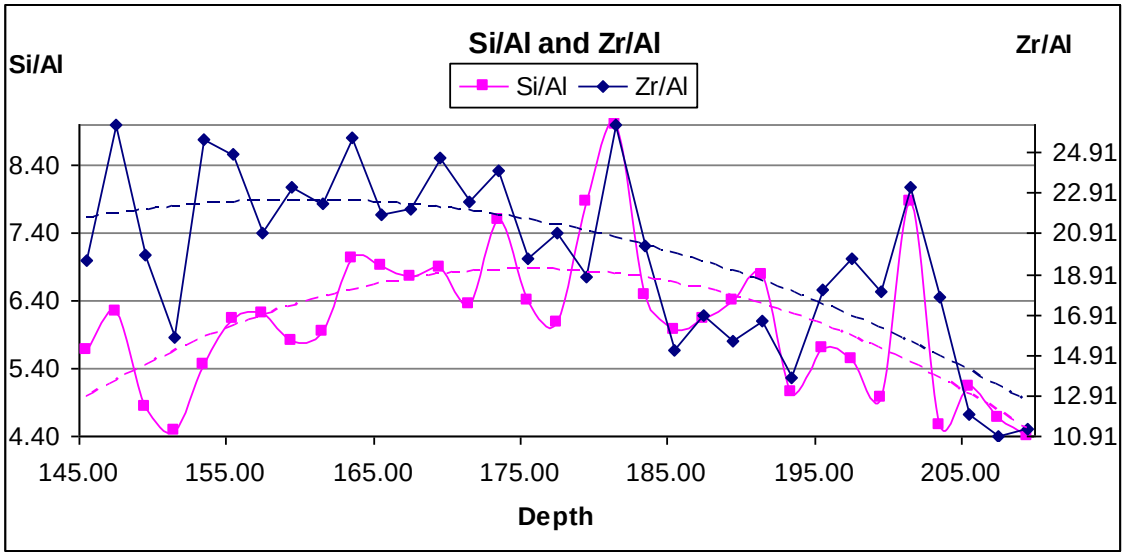

Fig. 4.2-2
This figure shows variability between different silt indicators normalised by Al. The trendlines highlighting the long term behaviour are second order polynomial

The next figure, **fig. 4.2-3**, reveals that the titanium normalised zirconium also changes toward higher values from a depth of 205 m upwards. Interestingly, the overall trend is very similar to the aluminium normalised zircon, at the same time, the logs are not identical and Ti/Al is therefore variable as well. The major discrepancies occur at 147.5, 163.5, 169.5, 173.5 and 201.5 m. There appears to be a short three point rhythmicity in Zr/Al ratio.

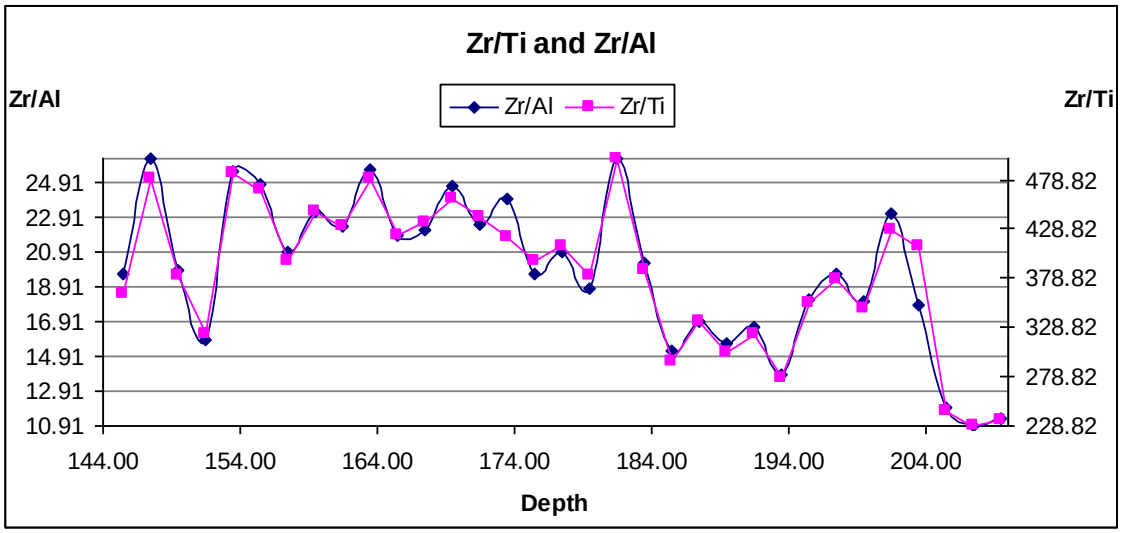

Fig. 4.2-3
Element ratios on depths 145 to 210.

4.2.1.1.3 T:M ratio

The plot of T:M palynomorphs to depth shows a strong variability reaching as much as 0.45 value signalling that there is twice as much marine than terrestric palynomorphs in the sample; this should be considered of very high value since the mean for the entire interval is 0.17. The overall trend is decreasing in value with a pronounced local variability, see **fig. 4.2-4,** the most striking local maxima are at 203.5, 181.5, 175.5, 171.5 but others occur at 193.5 and 159.5.

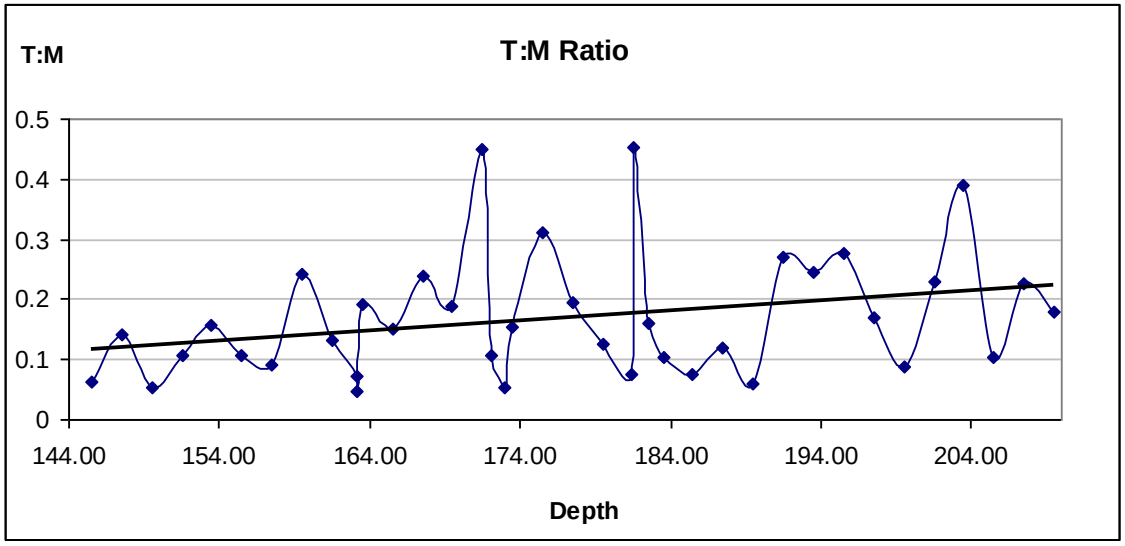

Fig. 4.2-4
Terrestric/Marine palynomorphs ratio on depths 145 to 210 m. See text in chapter above for further description.

4.2.1.2 New Data

4.2.1.2.1 Grayscale

The grayscale data is by far the most detailed curve achieved with theoretical precision of one millimetre and the maximum measured deviation of five centimetres, due to data processing. There are three orders of variability visible in the dataset, **see fig. 4.2-5**.

First are the very short-term excursions towards lighter values observable from the depth 184 m upwards, with a typical difference of 40 in value on the grayscale axis and an abrupt change over three consecutive points.

The second order variation is highlighted by the five point running mean curve with a typical oscillation of between 15 and 30.

The third order variability achieves a maxima of around 180-184.5 m and a minima between 145-149 m with numerical differences of 65, without the added short-term trends. Smaller, yet prominent is a local maximum of 152-156 m and a continuous decreasing trend from 184.5 culminates in local minima at 200 m.

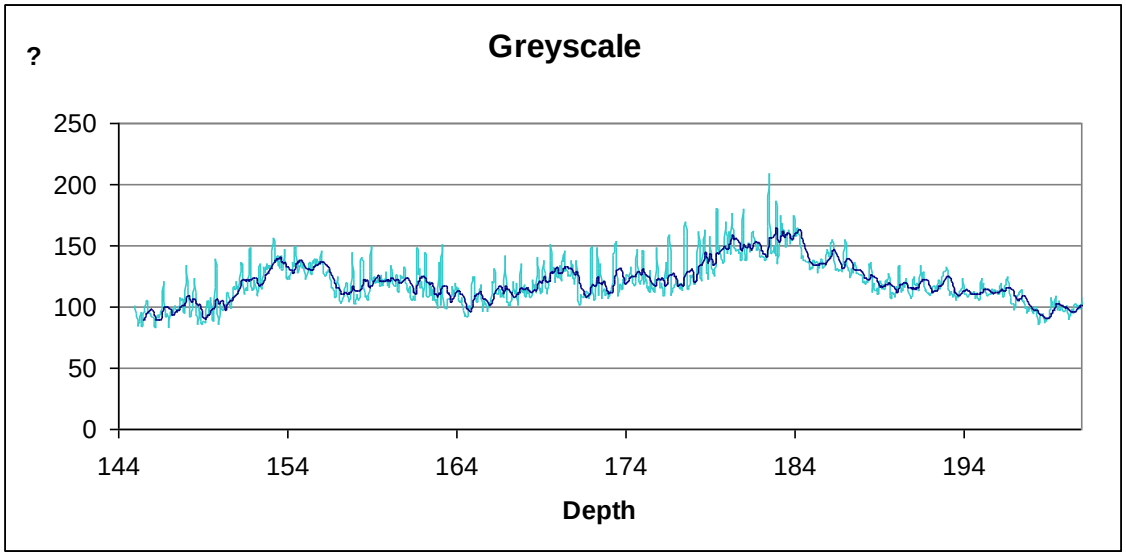

Fig 4.2-5

Presents the greyscale variability log, the higher the y axis number, the lighter the lithology. Data in the picture are in fact a running mean values for every 5 cm re-sampled in 5 cm intervals since the original dataset was too dense for this type of display. This is a great advantage later on when comparing these values to other datasets as no interpolation has to be made to achieve corresponding sampling intervals. It also eliminates some of the fluctuations reflecting the bioturbation colour changes. See text in chapter above for further information.

4.2.1.2.2 Magnetic Susceptibility

With the maximum measured value of $128*10^{-6}$ and relative error of 3 % any departure in value exceeding $4*10^{-6}$ can be considered significant. Three orders of MS variability can be observed, see **fig. 4.2-6**.

The third order displays visible maxima around 200-202 m and the two minima at 155-158 m and 178-184 m with a difference of $70*10^{-6}$.

The second order variability highlighted rhythmic behaviour of the trend without the superimposed first order low values, showing several ups and downs in approximately four metre intervals with a variability of about $20*10^{-6}$, for example, the local maximum at 173 m followed by the local minimum at 174 m.

The first order variability is exhibited as abrupt shifts over two successive reading points of about $46*10^{-6}$ towards lower values.

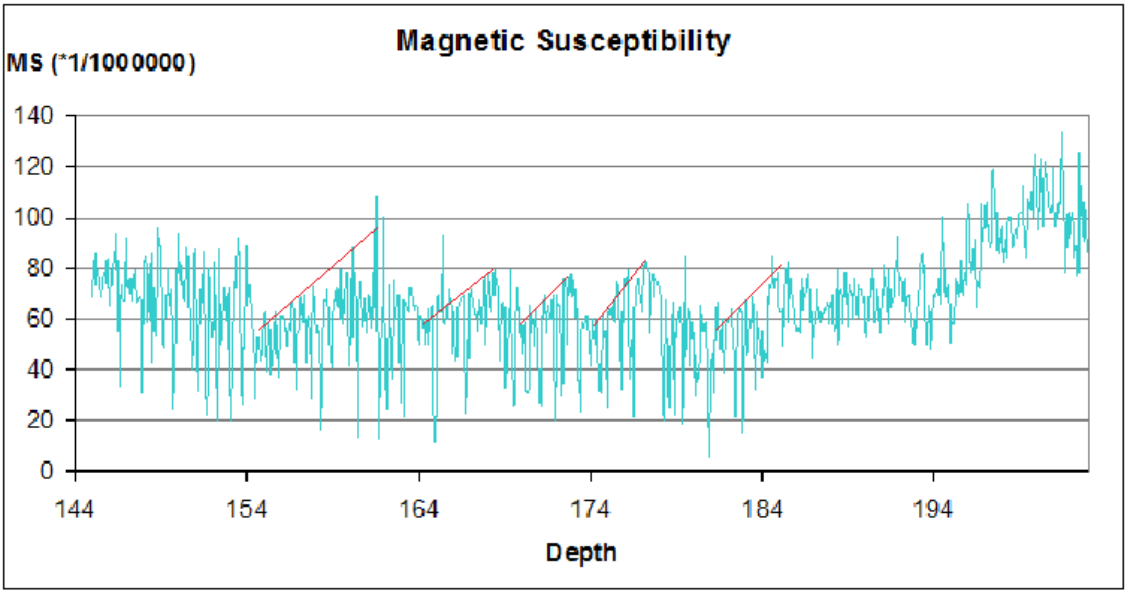

Fig. 4.2-6
Magnetic susceptibility log between depths 145 and 203 m showing approximate position of the second order variability. MS is the second most densely covered parameter along the Bch-1 core.

4.2.1.2.3 New geochemistry measurements

Tab.3

This table shows measurements of the handheld Niton spectrometer on selected samples. This dataset was chosen to reproduce the change in element ratios observed over the TUR 5 and TUR 6 boundary, as well as the small variability between Lithotypes II and III. Only the latter measurements were used for the purpose of this thesis in the end, the rest remains as a reference for corresponding measurements on other profiles in the basin which are to be performed at later stages of research. Note that the trend towards higher carbonate content was duplicated.

Depth [m]	Lithotype	Si [%]	Ti [%]	Zr [%]	Al [%]	Ca [%]
147.8	II	19.3	0.139	0.017	3.16	21.3
148	III	7.5	0.051	0.007	1.48	36.7
158.5	III	9.4	0.058	0.009	1.72	34.8
158.75	II	18.9	0.160	0.015	4.11	21.6
171.85	II	22.8	0.188	0.016	4.26	16.4
172	III	13.8	0.093	0.011	2.64	29.2
172.94	II	23.2	0.181	0.017	3.72	15.8
186.3	I	22.3	0.158	0.016	3.70	18.9
186.7	I	23.3	0.186	0.018	4.22	16.6
187	I	17.0	0.106	0.012	3.03	25.7
202	0	24.5	0.251	0.021	4.62	13.0
209.5	0	23.7	0.218	0.025	5.54	14.2
220.5	0	16.3	0.131	0.009	3.69	24.5

Tab.3 shows the percentages for calcium, silica, aluminium, zirconium and titanium acquired by the handheld Niton spectrometer; these were used as complementary information to the ICP dataset to investigate short-term variability.

For the results of other MS methods leading to signal decoding and Niton measurements calibration and evaluation, please see the following chapter. An effort to divide the pure data from their interpretation has been made, however, since this thesis involves two levels of data evaluation it seemed appropriate and less confusing to keep some of the relevant information and figures together.

4.3 Primary interpretation

The goal of this chapter is to introduce the above presented datasets in the light of information gained through petrologic investigation and identifying the dominant signal carriers for each dataset.

4.3.1 Geochemistry

The minerals and size fractions observed in thin sections can be divided into five groups based on their possible inferred contribution to measured Ca, Si, Al, Zr and Ti element concentrations. Their lists of decreasing probable shares are summed up in the table **Tab.4** together, in relation to either muddy or silty or coarser fractions.

Ca	**Si**	**Al**	**Ti**	**Zr**
Micrite (M) *Sparite (O)* *Bioclasts (C)*	*Quartz (S)* *Clay (M)*	*Clay (M)*	*Titanite (S)* *Rutile (S)*	*Zircon (S)*

Tab.4

This table shows the main carriers for each of the elements based on the micropetrology study of thin-sections and their grain size affiliation: S – silt, M-mud, C-coarser than sand, O-other.

4.3.1.1 Carbonate content

Based on the information above, it can be postulated that the carbonate content reflects the amount of micrite and bioclasts in the sample and complements the amount of siliciclastic fraction. It represents the highest possible value of micrite mud fraction and since the coarse bioclastic volume is rather low, it is a good proxy for the micrite amount.

This allows a rough estimate of clay mineral in the matrix from thin sections, for example, thin sections at 171.85 m display 64 % of matrix and the carbonate content is 48 % and the estimate of clay mineral content minimum is 16 %. When performed for

all nine samples that have this information available, the results show that carbonate dominates in Lithotype III, whereas in Lithotype II the siliciclastic content is generally higher with variable clay to silt ratio and one sample reaching over the fifty percent boundary. The one Lithotype 0 sample confirms the assumption of the lithology being less carbonatic as the clay content alone reaches over 45 % which is more than any other sample.

The short-term positive excursions most probably reflect the Lithotype III high sparite content; see Niton measurements over the couplets for comparison **fig. 4.3-1**.

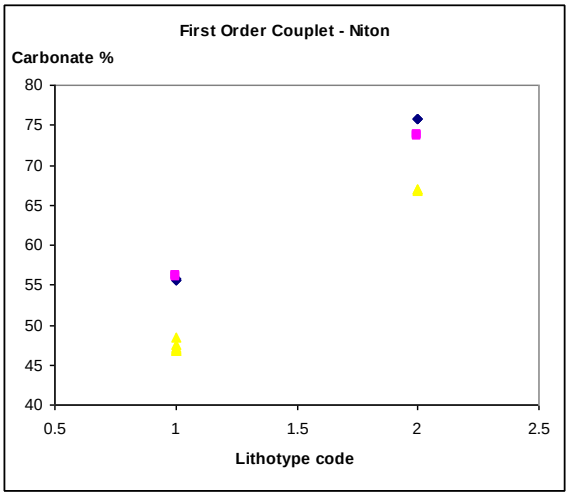

Fig 4.3-1
Showing variability of carbonate percentage change over the Lithotype II and III couplets. Three couplets were measured. Coding of 1 for Lithotype II and 2 for Lithotype III was used to facilitate easy comparison between different depths. Generally said any sample reaching over 60 % carbonate is likely to be a Lithotype III.

4.3.1.2 Element ratios

The long-term discrepancy in silica and zirconium ratios could only signify a long-term change in the Zr/Si ratio, see **fig. 4.3-2**, which can be explained only by either progressive zirconium enrichment of the lithology or quartz depletion. This means that different size fractions have to be in play as carriers of Zr and Si in order to differently react to the identical environment conditions or mixing the two sources one richer in zircon and the other in silica occurs.

The variability of the Ti/Al ratio signifies that some of the titanium is indeed carried in a different fraction than aluminium. The assumption that titanium in titanite and rutile is part of the small silty fraction as opposed to aluminium in clay is therefore validated.

The fact that Al and Ti normalised zirconium have the same long-term trend points towards a very similar behaviour of Al and Ti carriers with respect to the zirconium carriers. The same observation is true for Si/Al and Si/Ti. This is especially interesting since titanite and rutile are indisputably part of the silty fraction in all Lithotypes. This

could mean two possible scenarios, either the clay source is linked to that of titanite, or the mechanism responsible for the differential transport of clay to silt could also transport the smaller titanium bearing fraction.

The differences between Lithotype II and III are shown on the calibrated Niton measurements. The element ratios are variable, signalling some changes in the clastic component content; the selected couplets however have little in common. The only systematic shift between Lithotype II and III are in the Zr/Ti ratio, see **fig. 4.3-2**. The Lithotype II and III do not display any particular behaviour in terms of element ratios. The Lithotype 0 is characterised by a decrease in all ratios.

Lithotype I and Lithotype II overall show similar XRF and ICP values, although there is a trend toward higher values in Lithotype II. This combined with the fact that Lithotype II has lower matrix percentages and similar bioclast volumes leads to the inevitable conclusion that the matrix of Lithotype II contains lower clay/micrite ratio than Lithotype I and is therefore more carbonatic.

Using the same reasoning, the carbonate minimum for Lithotype 0 or at least its 200 – 204 m part probably reflects that this Lithotype has the highest amount of clay minerals in matrix.

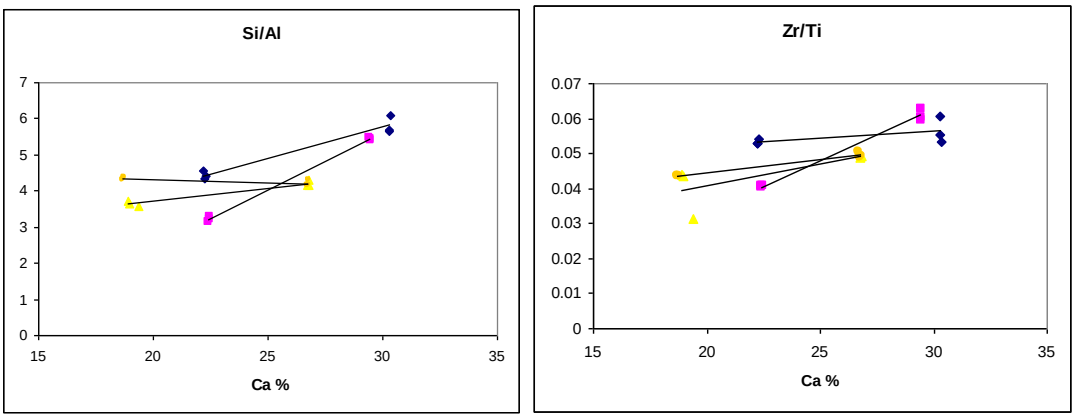

Fig 4.3-2
Figures showing element ratios to carbonate content for the three sampled couplets. Lithotype III always has higher carbonate content than Lithotype II. The pink couplet has Lithotype II value from below Lithotype III, the blue has Lithotype II value from above Lithotype III and yellows couplet has measurement from both below and above Lithotype III. There are two types of behaviour over the couplet for different element ratios
A all couplets show the same relative trend in different measure like in Zr/Ti or Si/Al ratio
B the couplets show differet relative trends over the couplet as in Zr/Al and Ti/Al ratio

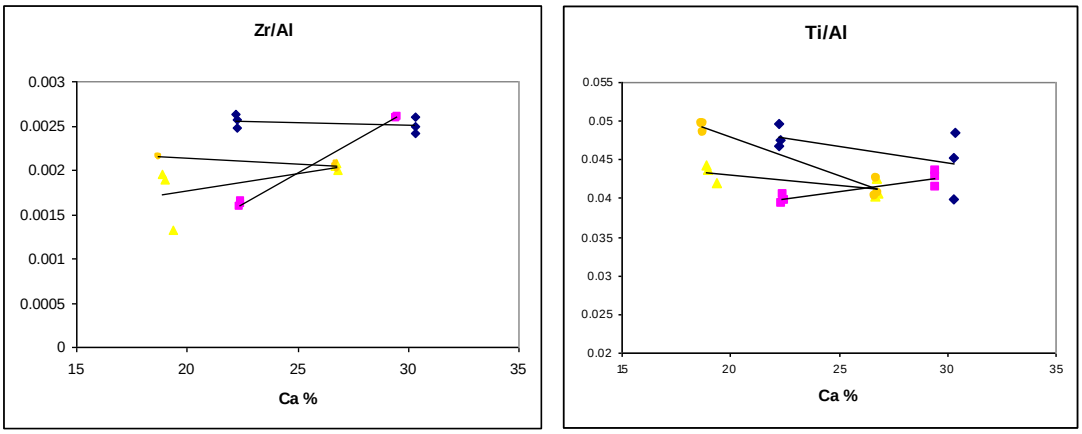

4.3.2 T:M ratio

This property can be viewed as an indication of either marine productivity, or terrestric input variation.

Neither short nor long-term trend seems to reflect any of the Lithotype 0 - III differentiation, although an abrupt increase in T:M visible in **fig. 2.3-1** could be assigned to the difference between Lithotype 0 and the rest of the core.

4.3.3 Grayscale

In the studied sediment, several constituents are likely to influence the grayscale value at each point of the core. Even a low percentage difference in organic component and pyrite tend to make the sediment substantially darker (*Tucker, 2001*); adversely calcite tends to make the lithology lighter (*e.g. Koptíková et al., 2010; Ortiz & O'Connell, 2004*) in our case this goes for both micrite and sparite. Also quartz grains could cause a drift to lighter values especially when compared to the muddy matrix.

The first-order variability reflects the Lithotype II and III variations. The second-order variability does not fit any of the pre-defined lithotype changes and occurs throughout the core, possibly less pronounced towards 198 m. The third-order trend is unlike anything reflected by the Lithotype definition, although a change of trend occurs between Lithotype I and II. The record is too short to effectively display changes towards Lithotype 0.

4.3.4 Magnetic Susceptibility

The nature of MS carriers could be identified by several lines of investigation, making it one of the most reliable interpretations.

The temperature variations of MS; see **fig. 4.3-3**, have in most cases revealed a strong hyperbolic shape, signalling the dominance of the paramagnetic MS carriers. Most of the samples displayed neither a Verwey transition of magnetite nor a Morin transition of hematite. In the six specimens the hyperbolic fits was worse and in some of them a very weak Morin transition could be identified, see **fig. 4.3-4.** However, even in these specimens the amounts of ferromagnetic minerals are very low being on the edge of detection. The method by Hrouda *(1994)* is used to resolve the rock MS into different components and it confirms the result of paramagnetic dominance, where the calculated hyperbolic values show a good fit to the measured MS, see **fig. 4.3-5**.

The Maximum Theoretical Paramagnetic Susceptibility was calculated from the ICP chemical analyses and compared to the Kappameter corrected MS. The values correlate reasonably (with R squared = 0.55) but the MTPS is higher than the measured MS. This evidently results from the fact that the ICP analysis provides only information on total iron content, not separated into Fe^{2+} and Fe^{3+} components, so when all iron is considered as trivalent, the MTPS gets higher. This line of evidence also points towards the dominance of paramagnetic MS carriers.

The paramagnetics in the core include clay, glauconite, pyrite, muscovite, hornblende and accessories such as titanite, rutile, tourmaline and zircon. Based on our knowledge of chemical compositions and MS values for the observed minerals, a simplistic model could be employed to ascertain which of the paramagnetic constituents is responsible for majority of the signal. The only viable solution is that the clay minerals are MS carriers, since they are the only fraction present in sufficient percentage.

The first-order variability follows the Lithotype II and III rhythms, the second order variability is obvious only in Lithotype II and the third-order variability does not match any of the predefined Lithotype variations, although the dataset is too short to reveal the Lithotype 0 behaviour.

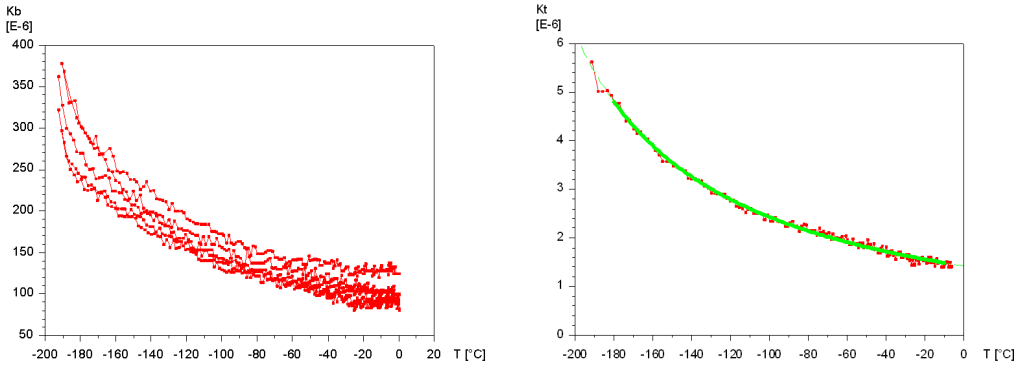

Fig 4.3-3

a)samples showing hyperbolic evolution of MS with temperature
b)demonstration of nice hyperbolic fit , although the computed hyperbola does show some y axis shift indicating a that some ferromagnetic minerals are present, only in very low amounts

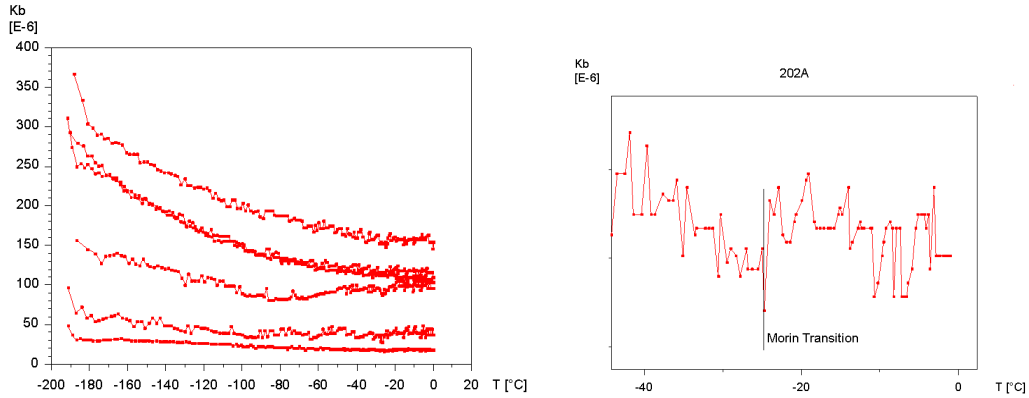

Fig 4.3-4

The six specimen showing worse hyperbola fits and showing a faint Moring transition indication of magnetite presence. The bad hyperbolic fit is most likely the result of very low MS value altogether, given to the fact that these samples are of the the Lithology III and therefore should contain mainly diamagnetic sparite.

Fig 4.3-5

Showing correlation between paramagnetic component and total measured MS on the control samples. No such correlation was revealed by an analogous diamagnetic + ferromagnetic fraction versus measured MS, therefore one can conclude that the variation in susceptibility is controlled by the variation in contribution of paramagnetic fraction such as clay minerals or mafic silicates.

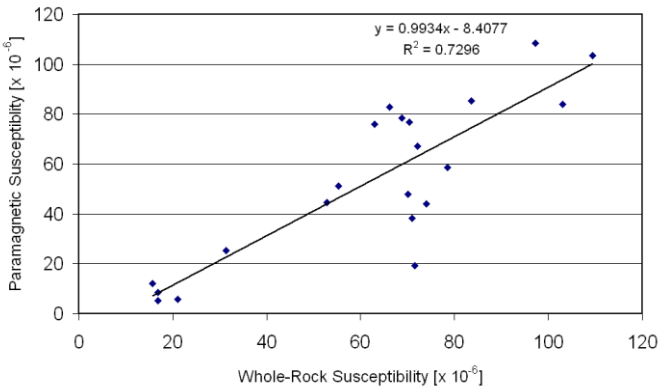

4.4 The Nature of Data Variability

The datasets described above have displayed at least three orders of variability over the studied interval. A frequency analysis tool was used to asses and characterise the data variability from the acquired MS and densitometry logs. In order to evaluate any cyclicity, the depth-to-time transformation has to be established for the interval, this

was performed with a combination of an independent sedimentation rate model and orbital tuning.

4.4.1 Sedimentation rate model

Sedimentation rate estimates can be calculated using biostratigraphic and carbon-isotope markers (*Uličný et al., submitted*) and an independent orbital age model adopted from the south-western part of the basin (*Laurin et al., in prep.*). The biostratigraphic and isotope markers link the Bch-1 core to a floating time scale of the orbital model. The thicknesses of strata bracketed by these markers are then used to calculate average sedimentation rates. As this tool became available it transpired that the observed rhythmic phenomena between Lithotype II and III are in fact much faster than any Milankovitch frequencies. For more information on the sedimentation rate model see **appendix 4**.

4.4.2 Orbital tuning

When the studied datasets were re-examined with the sedimentation model, the importance of second-order variability in susceptibility was revealed. With a recurrence in approximately 4 m and a long-term sedimentation rate of around 16 cm/kyr, the period of such a cycle would be approximately 25 kyr. This frequency is notably similar to the Milankovitch precession signal also observed in the Upper Turonian of the Úpohlavy quarry (*Laurin and Uličný, 2004*). Once the recurrence of this signal is statistically confirmed, tuning the dataset to the expected length of 22 kyr is substantiated.

MS bears information on the clay mineral content; it is therefore likely that this cyclic feature would show on a resistivity log, as it also reflects the relative amount of clay minerals. The approximately four to five metre cycles were identified on the resistivity log, leading into the two important outcomes. Firstly, the orbital tuning can be performed on a different and longer dataset, providing a somewhat independent source of depth-to-time conversion, to avoid circular reference (*Hinnov, 2000*). Secondly, the continuity of the observed cyclicity within the basin, once confirmed, can be ascertained.

The potential frequencies carrying precession and eccentricity signals were revealed by EHA, see **fig. 4.4-1**, and were used for transforming the depth series of MS and Grayscale into orbitally-tuned time-series for further investigation. This is performed by

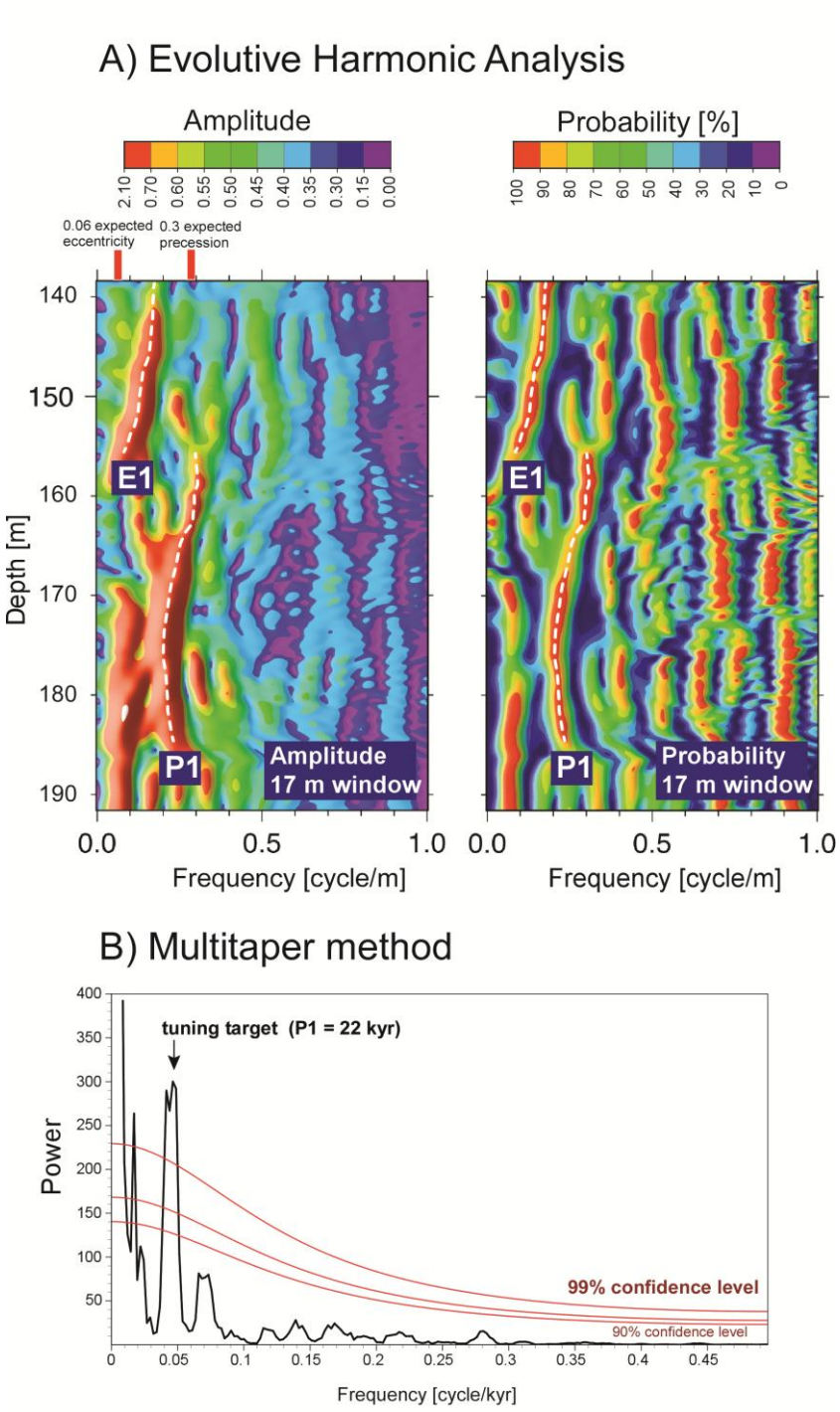

Fig. 4.4-1

This figure shows the results of time series analysis of the resistivity log based on which the MS and grayscale data was tuned.

A) Shows the results of Evolutive Harmonic Analysis with a 17 m moving-window and the associated independent significance F-test (probability in percent). Only the maxima in both amplitude and probability are considered for orbital tuning and due to the two crests of high amplitudes around 0.1 cycles per meter and O.25 cycles per meter are good candidates for the Milankovitch exccentricity and precessional signal.

B) The multitaper spectral estimate of the tuned resistivity, which is a check on the calculated sedimentation rates as the peak in precession became more pronounced and narrower. The fact that it reached over 99% confidence level is taken for a confirmation of successful orbital tuning.

using the frequency reading from each depth to calculate the expected sedimentation rate and ultimately the time interval between the two successive depths.

The hypothesis that the signal is precessional is supported by the fact that the mean sedimentation rates for the interval gives a value of 16 cm/kyr, which is a number close to the sedimentation rate model, and for comparison with the derived sedimentation rates; see **fig. 4.4-2**. If, for example, the obliquity signal was applied to the prominent frequency a shift towards lower values, around 10 cm/kyr would occur.

The orbitally tuned sedimentation rate is in agreement with a proposed slow down towards the top of the interval based on other lines of evidence already discussed in the Lithology description chapter.

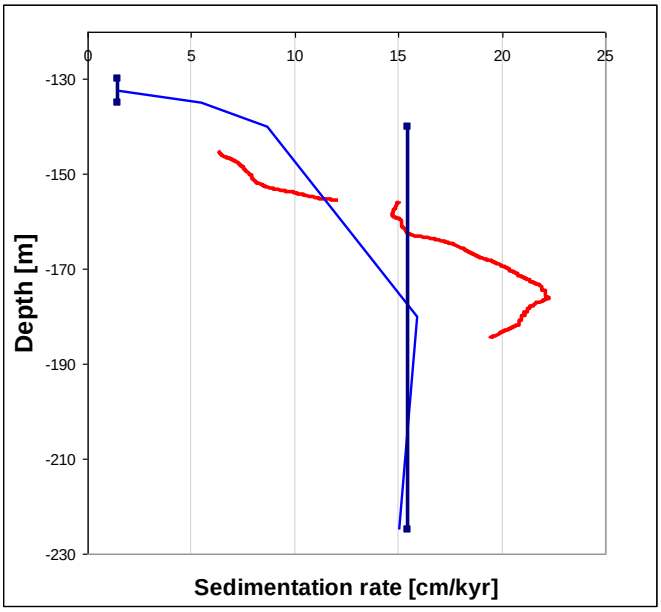

Fig 4.4-2
Comparison of sedimentation rate computed for the interval correlated to linear sedimentation speed models. The new sedimentation speeds are closer to the long term trend (blue) suggesting an abrupt, non-linear speed-up of sedimentation between FO-M.scupini and scupini acme at 140-135 m or possibly a problem in their respective position.

4.4.3 Results

The MS and grayscale data when inspected by EHA show similar images to resistivity see **appendix 5,** with a number of superimposed faster frequencies, as observed in the core lithology. Once tuned, the multitaper evaluation of the MS reveals a quasi-periodic nature of the short-term cyclicity or what has been described as first-order variability, see **fig. 4.4-3**, this is also true for the grayscale dataset.

There are three orders of cyclicity revealed by the Frequency analysis which are Cycle I, Cycle II and Cycle III and these were identified as eccentricity (95 kyr), precession (22 kyr) and short-term (1.6 and 3.3 kyr) millennial cycles. The first two occur over

Lithotype II and are interpreted as being governed by orbital control. The shortest variability is a quasi-periodic process characterised by Lithotype II and III rhythmicity.

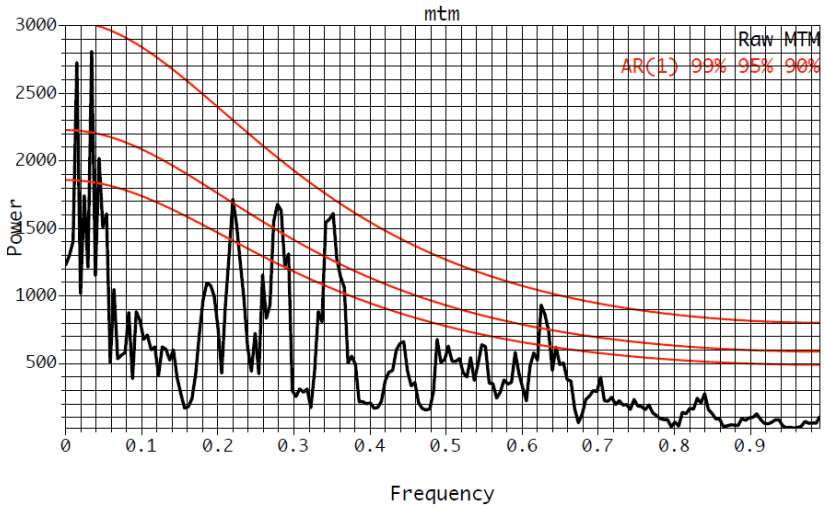

Fig 4.4-3
The results of multitaper investigation of orbitally tuned MS signal showing peaks for 3.3 and 1.6 kyr cyclicity as well as the by the eccentricity and obliquity peak.at the lower frequencies. The confidence levels displayed by red lines are of 90, 95 and 99 % confidence level. Generally anything above 95% can be considered a good indication of not belonging to red noise.

Short-term variability is not merely a display of harmonics in the evaluation process, as real variability is observed in the core. The probability of this cyclicity being real-system harmonics of the Milankovitch precession is not likely because their numeric value does not correspond with 3rd nor 4th order harmonics, nor is it likely to have such a strong signal in the sediment (*Weedon, 2003*).

4.5 Multi-proxy analysis

The major change in sedimentary conditions at the base of the interval visible from long-term trends, see **fig. 2.3-1**, and the three orders of Cyclicity (I, II and III) will be evaluated using the multi-proxy approach. Paleoclimatologic interpretations should preferrably be based on a carefully designed, multiproxy approach (*Bábek et al., 2011a*)

4.5.1 General assumptions

The siliciclastic sediment, both silt and clay was transported in suspension into the distal parts of the shallow water basin where it was deposited. No evidence of any other transport mechanism was documented and these processes are considered dominant for distal sedimentation (*Nichols, 2009*). The grain size reflects the energy of the environment both at the site of input and during deposition (*e.g. Bábek et al., 2011b*)

The availability of the siliciclastics in distal paths of the basin can be governed by the variability in sediment supply due to weathering, proximity of source and transport direction paths. In the case of one sediment source, it is generally expected that the heavier and larger grains are deposited near the shore while smaller and more mobile

particles are carried further. In such a scenario, the silt/clay ratio and corresponding element ratios are expected to decrease the basin ward.

However, the bimodal grain size distribution in the sediment signals a more complicated scenario and two different mechanisms of getting the grains into suspension must have been at play. Both scenarios, with one source area or two separate sources have to be considered

The primary productivity and corresponding carbonate content is expected to reflect in situ sedimentary conditions.

4.5.2 Base of TUR 6

Is characterised by the difference between Lithotype 0 and Lithotypes I + II and reflects a secular change in long-term development in the Bch-1 core towards a more carbonatic lithology.

It is characterised by an onset in coarser siliciclastic sedimentation as seen from the element ratios and grain size changes. The Ti/Al, Zr/Al and Si/Al ratios displays a pronounced one step shift, yet the carbonate content also shows an increasing tendency. The silt/clay ratio rises dramatically and the relative clay content decreases steadily from the onset of TUR 6 as observed on the MS log. The high T:M ratio over an interval is probably a reflection of the increase in influx from land.

4.5.2.1 Interpretation

The increased amount of carbonate in the matrix most probably reflects an increase in the biogenic productivity at the onset of TUR 6. The depositional environment must have been rather low energy as the very fine micrite and some clay were allowed to settle. The onset of carbonate production is not likely to be a reflection of a mere transgression, however, as this does not account for the increased silt influx or the relative decrease in clay component. The decrease in clay content could theoretically be a mere effect of dilution by matching the amount of carbonate and silt but should manifest in a rapid increase in sedimentation rate which is contradicted by the tuned sedimentation rate model. The case that less clay was available is the more probable scenario and possibly the only solution. It is difficult to imagine differential change in weathering that would cause an increase in coarser but decrease in clayey siliciclastic fraction. A coincident change in the pathway of clay distribution, silt source proximity and the onset of higher bioproductivity is proposed (see discussion).

4.5.3 Cyclicity I

Cyclicity I is reflected in the third order signal of MS and grayscale datasets between 145 and 184 m and is the least explored of the variations, as it was not uncovered until late on and therefore not specifically targeted by any of the additional sampling.

It is partly displayed as in the broad local maxima in the carbonate content and lower values in T:M ratio. For the long-term correlation of MS with ICP aluminium and Grayscale with XRF carbonate, which further justifies the use of these datasets for time-series analysis of the succession.

4.5.3.1 MS

The Cyclicity I is reflected in the third order variability trend by all clues connected to siliciclastic fraction, probably clay. The long-term minima in the trend is the most likely place of high carbonate or quartz silt content.

4.5.3.2 Grayscale

In grayscale the signal is most likely to not be overly dependent on the amount of organic matter or pyrite as they both decrease over the Lithotype I, yet the log shows gradual darkening, nor the amount of sparite because it is if anything higher in Lithotype I than in Lithotype II. This leads to a conclusion that long-term value is in some way connected with the amount of micrite to siliciclastic content/clay ratio. The two broad maxima around 154 and 184 m would then be areas of high micrite amount.

4.5.3.3 Interpretation

Cyclicity I is possibly reflected by the two somewhat independent processes which are being observed, that is the changes in productivity observed on the grayscale and carbonate log and the coincident with eccentricity forcing and a longer term variability of sediment input reflected in MS and element ratios. The grayscale maximum around 154 m carries is accompanied in an abrupt shift towards more clay rich interval on MS at 154 m and a decrease in T:M and Si/Al at 147.5 m. This sequence of observations could bear a link to long-term T-R history. A similar but less prominent maximum in carbonate occurs around 184 m and is also accompanied by a change in siliciclastic proxies.

4.5.4 Cyclicity II

Was defined within the Lithotype II and is characterised by second-order variability on the inspected datasets. As this variability was not originally observed on the core, it is very likely to be connected to the matrix composition, possibly the clay/micrite ratio.

4.5.4.1 Grayscale

The second order variability could reflect anything from the amount of carbonate, recrystallisation of matrix index, the amount of pyrite due to redox conditions or different clay/micrite ratio. The amount of quartz silt does not play a dominant role as the more clastic intervals of 147.5 and 171.5 do not display any significant deviation towards higher values.

4.5.4.2 MS

The second order MS variability does not dramatically react to the amount of quartz silt as the pronounced maxima of 147.6 and 171.5 m are not particularly highlighted by the MS log. When the possibility of differentiation in the magnetite diagenesis is overlooked, the only other possible explanation is that of the changing clay content by short-term variations of the clay to micrite ratio in matrix.

4.5.4.3 Geochemistry

The differentiation between the second and third order variability observed in MS and grayscale, is not straightforward in the carbonate content datasets which can be either caused by the "under-sampling" of the second order variability; another possible explanation is that the long-term variability is much higher in magnitude, which would point towards the two mechanisms governing this variation (e.g. long-term changes in productivity and short-term mixing of siliciclastic and carbonate material).

A high variability of all element proxy ratios is, by all clues, connected to the Cyclicity II but no correspondence to MS or the grayscale value has been discovered by statistical treatment.

4.5.4.4 Interpretation

A good correlation exists between MS and a great number of ICP aluminium measurements, yet no such behaviour is observed when comparing to carbonate content. This can be explained by a three component system where all, quartz silt, clay and carbonate matrix component vary over time. This interplay of siliciclastic dilution,

accompanied by bioproductivity on the Milankovitch timescale can ensue from various sedimentary scenarios.

4.5.5 Cyclicity III

Short-term variability is displayed pronouncedly on both MS and Grayscale datasets and is the best documented variation over the core. It is a quasi-periodic feature with frequencies of 1.5 and 3.3 ka. The information gained for Lithotype II and III variability applies to this cyclicity.

4.5.5.1 Magnetic susceptibility

The MS value excursions are easily explained through the occurrence of diagenetic spar. Early cementation of the sediment prevented further compaction and therefore limited the amount of any paramagnetic minerals per volume. The numeric value of the MS probably depends on the width of inspected Lithotype III layer.

4.5.5.2 Grayscale

The grayscale data reacts sensitively to the high sparite content in the Lithotype III, although the ensuing smaller amounts of dark constituents such as pyrite and organics per volume could amplify this effect. The information reflected in the log is mainly that of a different diagenetic history.

4.5.5.3 Geochemistry

The Zr/Ti ratio reveals a relationship that is in stark contrast with microscope observation, see **fig. b** (in interpretation 1). The decrease in the grain size is expected to be accompanied by relative titanium increase in respect to zirconium. This could only be explained by the winnowing of finer grain size in Lithotype III when compared to the Lithotype II situation.

The Si/Al ratio changes confirms the fine fraction winnowing to a certain extent, with only one couplet value not displaying this behaviour. Both Zr/Al and Ti/Al randomly display both types of change towards lower and higher values between the Lithotypes.

This sort of variability between couplets can be viewed in two ways, either as reflecting the real state of sediment in which a complicated interplay between transport paths of different elements is to be expected or a discrepancy between relative calibrations of

data in which case only a vague assumption that fine fraction is being winnowed in Lithotype III can be established.

4.5.5.4 T:M

The Lithotype II and III variability targeted by the six additional data points did not show any systematic behaviour. Two out of three couplets display tendency towards lower T:M ratio in the Lithotype III. All couplets display a lower value (below 0.16) for both Lithotype II and III; this could mean the variations are characteristic for the times of lower terrestric input.

4.5.5.5 Interpretation

The early diagenetic overprint is acting to highlight a primary sedimentary signal as suggested by micropetrology and geochemistry observation. Cycles where secondary diagenesis enhanced other primary bedding rhythms has been described (*Arthur et al., 1986*). Although there is a possibility that the diagenetic signal is mixed and is only sometimes associated with original lithology variation, the periodicity acts more in support of the argument for a producing periodic signal but mere diagenesis is problematic (*Schwarzacher, 1993*).

The observation of T:M ratio does not imply increased productivity, and the overall higher carbonate is most likely a combination of early diagenetic enrichment during the sparite matrix recrystallisation so it cannot provide further information.

A process that would explain the decrease in clay content connected to overall silt grain size decrease would be difficult to find. This cannot be the case of a simple sea level rise nor can an increase in silt/clay ratio be accounted for, or as a mere change in clay distribution path. A complicated scenario of two competing feeding mechanisms between the two siliciclastic source areas or interplay of the two sedimentary mechanisms are to be expected, both reacting to the same external forcing and occurring in phase and repeatedly. One of the possible solutions would be a coeval change in water circulation pattern or strength with decrease in siliciclastic input either due to a rise in sea level or weathering effectiveness.

5 Discussion

The correlation of the Bch-1 core to the surrounding cores is essential when considering the spatial stability of the studied phenomena, which has a direct impact on their interpretation. These correlations to the north-west Lužice-Jizera Sub-basin and south-east Orlice-žďár Sub-basin were performed (*Uličný et al., submitted*) and from which the relative sea level change estimate was adopted. For details of the correlation, see **fig. 4.1-1**, which confirms the stability of the precessional Cycle II signal, as well as a hint of the millennial cyclicity although somewhat obscured by a low resolution of the logs.

5.1 Millennial cyclicity

The millennial cycles can be investigated using the tools designed for assessing the Milankovitch cyclicity variations. These cycles are most likely results of secondary depositional effects, as they do not reflect productivity or simple dilution properties; they are most likely connected to the variations in energy levels of the depositional environment.

The most fundamental question is whether the millennial variability is associated with internal processes inherent in the sedimentary system or ocean-atmosphere dynamics (*Munk et al., 2002*). This indeed is the much discussed question of autocyclicity versus allocyclicity, however, Schwarzacher (*1993*) pointed out that each periodic cycle is in fact allocyclic in origin as an external forcing is needed to create periodicity and discourage classification. A discussion of comparable millennial signals explored in other studies follows, as the interpretation faces the same dilemmas.

There is growing evidence for the environmental cycles with periods between one to ten thousand years (*for overview see Weedon, 2003*). The ice rafting Heinrich events and oscillations in temperature proxies called Dansgaard-Oeschger (DO) events and associated Bond cycles from the last Ice-Age are described with the best proxy record available for research. Moreover, the periodicity of circa 1.5 ka of the DO cyclicity is suspiciously similar to the observed Cyclicity III (*e.g. Munk et al., 2002*).

Many explanations have been offered for the occurrence of the DO but the general convergence is towards a stochastic resonance model (*Weedon, 2003*) which is a model where weak external periodic forcing is amplified by random noise, for example that of a high tide signal amplified by the interaction with ice sheets in the form of larger-than-usual ice-rafting event *(e.g. Berger & Rad, 2002).* The specifics of the signal transfer

are not delved into because the greenhouse climate could not provide the same feedbacks as proposed for the DO signal.

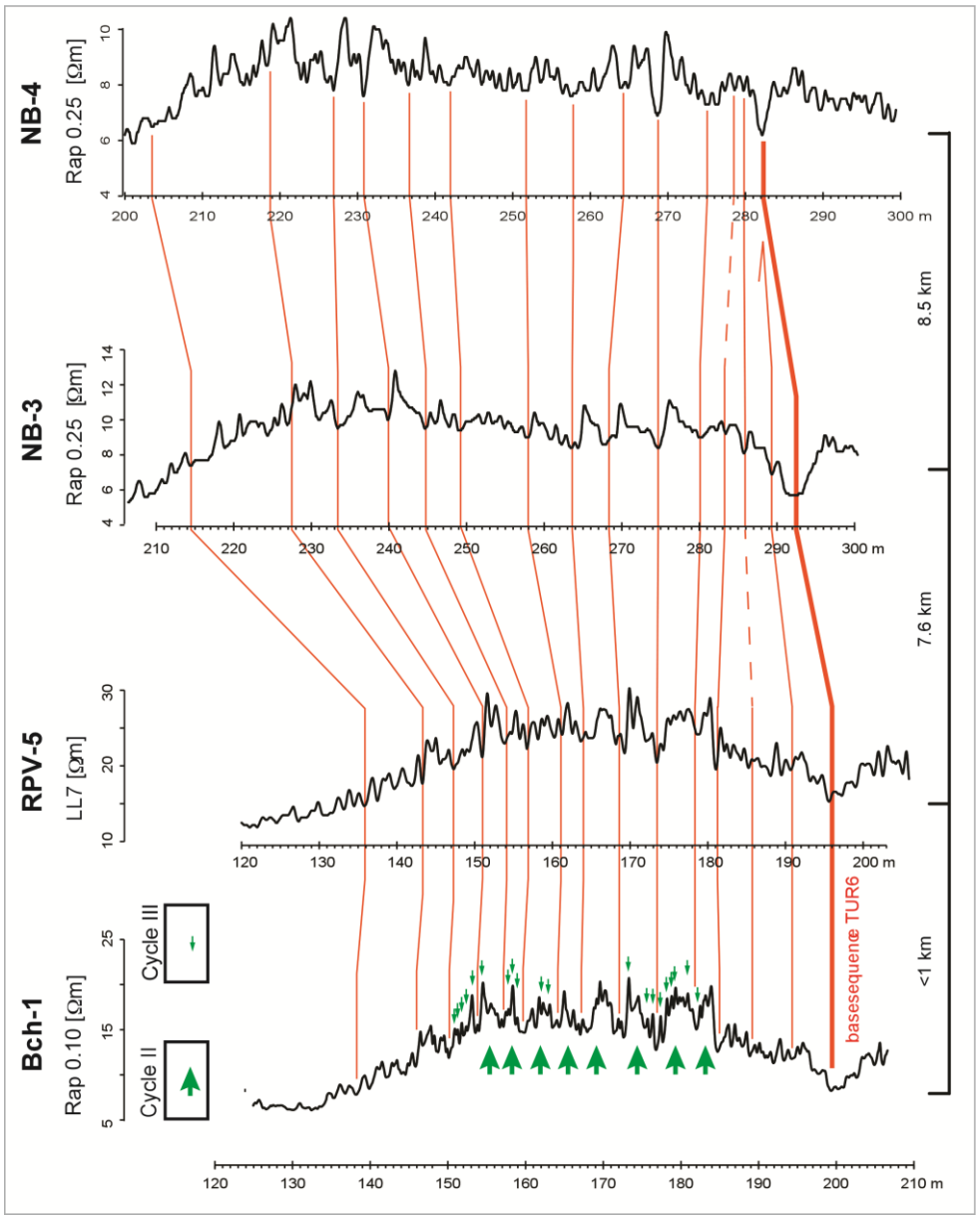

Fig 5.1-1
This figure displays correlation of the Bch-1 core resistivity log towards north east, for position of the respective cores see fig.2.2-1, the data was obtained from J.Laurin personal communication. The correlation of precessional Cyclicity II indicated by the big green arrows is well established and the millenial cyclicity is possibly displayed as indicated by the small green arrows.

Yet there is persistent power-spectra evidence for millennial-scale changes throughout the Paleozoic (*Weedon, 2003*). Milankovitch, solar and tidal origin or internal forcing of ocean-atmosphere system were all proposed as a possible cause for the millennial cyclicity, see Munk et al. (*2002*) for an overview. The case of lunar gravity forcing is especially appealing as it would be plausible even in the greenhouse

Cretaceous World and because the BCB is known to have been influenced by tides (*Mitchell et al., 2010*).

In our case the quasiperiodic cyclicity occurs mainly over the two eccentricity peaks in productivity. As the cyclicity most likely reflects changing terrigenous input conditions and since the rise and fall of the tides is accompanied by tidal currents that move water and sediment from place to place (*Garrett, 2003*), they could offer a viable explanation for the observed phenomena. The long periods between the occurrences between tide events, these have been explained by Berger & Rad (*2002*) who proposed that the maximum tidal activity had to fall into a narrow seasonal window to be geologically effective.

This line of thought is bordering on an over interpretation of the data at hand and is intended more as a line of deliberation with the potential for further study than a rigorous determination of the Cyclicity III origin. Variations in bottom sheer stress tied up with seasonality changes could, under certain conditions be similar.

5.2 Cyclicity II and Precession

The variations in Earth's orbital parameters are recorded in succession of TUR 6, therefore it must have been a part of a sensitive depositional system where the periodic external forcing is accompanied by cyclic changes in the environment resulting in regular changes in composition. As the variability can also be seen on the surrounding correlated cores and possibly in the south-western record in Úpohlavy quarry (*Laurin and Uličný, 2004*) and thus the phenomenon is of a whole basinal importance.

The variations in dilution and possibly productivity have been inferred from the MS and grayscale datasets and supported by the short-term variability of the element ratio proxies of siliciclastic flux. The reasoning is built on a similar base as used in Laurin & Vodrážka (*2010*) who also pointed out that the proximity of siliciclastic source should be interpreted in favour of dilution. Important changes in redox conditions or oxygenation levels can be ruled out, based on the presence of bioturbation.

From the processes meditating the signal transfer variations in runoff from the land, energy changes in strength of storms or sea level fluctuations are viable. In culminating greenhouse periods it is not likely that ice sheets were the driving mechanism, which is undermining the possibility of periodic global sea level fluctuations due to glacioeustasy. Although, similar hemipelagic bundles in the Úpohlavy quarry were tentatively interpreted as changes in siliciclastic flux that followed transgressive-

regressive events of the adjacent shoreline based on the architecture of sediment packages correlated to the siliciclastic margin (*Laurin & Uličný, 2004*). Since similar high-resolution architecture investigation was not performed on Bch-1 no evidence for this is present.

Changes in oceanic circulation and latitudinal migration of climatic belts cannot be ruled out as a cause but these seem to be on a too large scale and would have to be confirmed from other locations in at least European regional scale. On the other hand orbitally induced variations of tidal amplitude and tidal current strength are expected to have been stronger during greenhouse (*De Boer & Alexandre, 2012*) and could have acted in the case of the tide influenced BCB; from the climatic forcing the changes in precipitation, storminess and possibly also basin-wide circulation connected to the wind patterns are the most likely scenarios.

5.3 Cyclicity I and T: R history

The correlated long-term transgression-regression history seems to be in some agreement with the eccentricity paced maxima in productivity characterised by a greater amount of carbonate in the matrix. Especially with the onset of transgression around the 154 m it seems to correlate from the south-eastern Orlice-Žďár sub-basin and shows an increase in carbonate followed by a decrease in coarser siliciclastics.

The response of the siliciclastic ratios, however, somewhat lags the original signal, which could be the effect of a nonlinear response to the increased accommodation change as stated in Laurin & Vodrážka (*2010*) which could speak in favour of an eccentricity sea level forcing (*Laurin & Vodrážka, 2010*), although it has been argued that the response time of the siliciclastic system is expected to have been short due to the limited size of drainage basins (*Uličný et al., submitted*).

5.4 Base of TUR 6

The difference between TUR 5 and TUR 6 sedimentation in Bch-1 core was part of a basin wide change in conditions defined by the change from Jizera to Teplice Formation in the south-western part of the basin. The basin-wide transgression postulated in earlier studies (*e.g. Valečka & Skoček, 1990*) could not on its own be a cause for the increased coarse siliciclastic influx.

The observed phenomena could not possibly be only a reflection of local tectonic subsidence patterns, as a dramatic change occurred over a large part of the basin

(*Herčíke et al., 1999*). The coeval increase in carbonate production could not therefore be a result of decreased sediment supply.

This suggests that the phosphatic lag present in the Úpohlavy quarry was more likely a result of another means of slowing down of sedimentation rates (*Nichols, 2009*) such as condensed sections are likely to be the result of current or wave reworking (*Tucker, 2001*). This interpretation was proposed by Laurin & Uličný (*2004*) and is therefore corroborated by the along-stream deposits.

The coincident transgressive phase in the coarse siliciclastic accumulations was therefore most likely not an eustatic because there is not unequivocal proof of transgression in the hemipelagic settings, and it is more likely that the proposed tectonic reorganisation of the basin characterised by accelerated subsidence rates along the Labe-Železné Hory FZ (*e.g. Uličný et al., 2009*) was accompanied by more local changes in basin paleobathymetry. The accompanying water-mass circulation pattern changes suggested in Laurin & Uličný (*2004*) can explain all the observed phenomena - the shift in the accumulation areas and their relative advance in the south-eastern direction would explain the increase in siliciclastic flux and the increase in bed sheer stress resulting from the enhanced water mass circulation and would lead to the bypassing of some of the clay. Altogether, this theory cannot be disproved by the observations in the Bch-1 core.

The influx of boreal faunas and its coincidence with the culmination of the oxygen isotope excursion, interpreted to record climate-driven change in European water circulation, remains an intriguing coincidence.

6 Conclusions

This thesis was proposed to explore the subject of distal and hemipelagic sedimentation in the Bohemian Cretaceous Basin, which was recently re-opened for investigation in the light of modern geochemical and sedimentological approaches. The two years of work with the respective petrological, geophysical and geochemical datasets uncovered the potential and restraints of a combined multi-proxy approach and time-series analysis in distal fine-grained deposits, especially with respect to determining the origin of the different sediment fractions.

The results of the interpretation and general contributions can be summed up into three categories of increasing geological importance.

Firstly, there is a methodological value. The grayscale analysis was performed for the first time on Czech Cretaceous succession and an effective setup was constructed enabling accurate acquisition of grayscale logs from a core, the procedure once devised can be used on any number of samples across the whole lithologic spectrum. Also a magnetic susceptibility log was obtained from the same core followed by an effort to ascertain the magnetic susceptibility carriers. This could be easily applied on any hemipelagic strata. In this way, two variation curves represented by possibly different causes are obtained enabling an improved geological interpretation.

Secondly, for the use of the Bch-1 core investigation, some previously unnoticed phenomena were uncovered, such as preserved lamination and particularities in foraminiferal assemblages. The rigorous classification of lithologies was performed and an enhanced sedimentation rate model could be devised based on orbital tuning. A parallel interpretation of the water level oscillations was suggested which supports the basin-wide correlation results.

Lastly, the origin of the three orders of cyclicity was discussed. The millennial quasi-periodic variations in lithology were deposited in times of decreased coarse siliciclastic supply, accompanied by the increased bypassing of the clay sized fraction and were later highlighted by differential diagenesis. Cycles reflecting the Milankovitch precession frequencies were recorded in the clay content variability, most likely reflecting a mixed siliciclastic dilution and carbonate productivity signal. The longest period cyclicity was identified as an eccentricity signal and appears to reflect the changes in productivity with a superimposed sediment supply variation, possibly in beat

to the sea-level change. The secular onset of hemipelagic sedimentation was confirmed to reflect the changes in paleogeography, circulation and sediment dispersion.

The importance of tides and circulation pattern changes on a lithologic and geochemical character of the distal facies was repeatedly confirmed to highlight the necessity of caution when interpreting similar distal environments.

Although the full determination of the exact sedimentary history, mediating the translation of the Milankovitch frequencies into the Upper Turonian lithologies of the Bohemian Cretaceous Basin are beyond the scope of this study, the independent detection of the Milankovitch cyclicity, at new locations, contributes to a number of levels. It speaks in favour of the basin-wide nature of this phenomenon and is another piece of evidence adding to the growing list of studies that suggest the aptitude of the Late Cretaceous system to the transferring changes in orbital parameters into the sedimentary record.

The author realizes that it is the global-palaeoclimatic effects or even the astronomical forcing that are stressed in interpretation of the rhythmicity even though the other geological effects, such as Cretaceous plate tectonic motions etc., could also have played a role. A more extensive investigation based on correlation and other datasets would be needed to determine these effects with a certainty, it is believed that they will be studied in future works.

Overall, the nature of the short-term carbonatic lithology rhythmicity was revealed achieving the main goal of the study. Even though the conclusions were different from what was originally expected, the investigation has helped to reveal the Milankovitch signal in the Bch-1 succession and raised several new questions concerning the basin-wide circulation patterns in the Bohemian Cretaceous Basin and their relation to the global climate variability.

7 References

Adams, A.E., MacKenzie, W.S. and **Guilford, C.** (1984) Atlas of sedimentary rocks under the microscope. Wiley, Harlow, 104 pp.

Arthur, M.A, Bottjer, D.J., Dean, W.E., Fisher, A.G., Hattin, D.E., Kauffman, E.G., Pratt, L.M. and **Scholle, P.A.** (1986) Rhythmic bedding in Upper Cretaceous pelagic carbonate sequences: Varying sedimentary response to climatic forcing. *Geology*, **14**, 153-156.

Bábek, O., Chlachula, J. and **Grygar, T.M**. (2011a) Non-magnetic indicators of pedogenesis related to loess magnetic enhancement and depletion: Examples from the Czech Republic and southern Siberia. *Quaternary Science Reviews*, **30**, 967-979.

Bábek, O., Faměra, M., Hilscherová, K., Kalvoda, J., Dobrovolný, P., Sedláček, J., Machát, J. and **Holoubek, I.** (2011b) Geochemical traces of flood layers in the fluvial sedimentary archive; imprications for contamination history analyses. *Catena*, **87**, 281-290.

Berger, W.H. and **von Rad, U.** (2002) Decadal to millennial cyclicity in varves and turbidites from the Arabian Sea: hypothesis of tidal origin. *Global and Planetary Change*, **34**, 313-325.

Bice, K.L., Birgel, D., Meyers, P.A., Dahl, K.A., Hinrichs, K. and **Norris, R.D.** (2006) A multiple proxy and model study of Cretaceous upper ocean temperatures CO2 concentrations. *Paleoceanography*, **21**, 1-17.

Chang', S.B. and **Kirschvink, J.L.** (1989) Magnetofossils, the magnetization of sediments, and the evolution of magnetite biomineralization. *Annual Review of Earth and Planetary Sciences*, **17**, 169-195.

Chlupáč, I., Kovanda, J. and **Stráník, Z.** (2002) Geologická minulost České Republiky. Academia, Praha, 426 pp.

Čech, S. (1989) Upper Cretaceous Didymotis Events from Bohemia. In: *Cretaceous of the Western Tethys* (Ed. J. Wiedmann) pp. 657-676. Proceedings of the 3rd International Cretaceous Symposium, Tübingen 1987, Stuttgart.

Čech, S (2011) Palaeogeography and stratigraphy of the Bohemian Cretaceous Basin (Czech Republic) – and overview. In: *Geologické výzkumy na Moravě a ve Slezsku*, 1, 18-21.

Čech, S., Hradecká, L., Laurin, J., Štaffen, Z., Švábenická, L. and **Uličný, D.** (1996) Úpohlavy quarry: record of the late Turonian sea-level oscillations and synsedimentary tectonic activity. In: *Stratigraphy and Facies of the Bohemian-Saxonian Cretaceous Basin (Ed. T. Voigt)* Field trip guide, 5th International Cretaceous Symposium, pp. 32-42. Freiberg University of Mining and Technology, Freiberg.

Čech, S., Klein, V., Kříž, J. and **Valečka, J.** (1980) Revision of the Upper Cretaceous stratigraphy of the Bohemian Cretacous Basin. *Věstník ústředního ústavu geologického*, **55**, 227-296.

De Boer, P.L. and **Alexandre, J.T.** (2012) Orbitally forced sedimentary rhythms in the stratigraphic record: is there room for tidal forcing? *Sedimentology*, **59**, 379–392.

Dunlop, D.J. and **Özdemir, Ö.** (1997) Rock Magnetism. Fundamentals and Frontiers. Cambridge University Press, Cambridge, 573 pp.

Ellwood, B.B., Crick, R.E., Hassani, A.E., Benoist, S.L. and **Young, R.H.** (2000) Magnetosusceptibility event and cyclostratigraphy method applied to marine rocks: Detrital input versus carbonate productivity. *Geology*, **28**, 1135-1138.

Erba, E. (2004) Calcareous nannofossils and Mesozoic oceanic anoxic events. *Marine Micropaleontology*. **52**, 85-106.

Friedrich, O., Norris, R.D. and **Erbacher, J.** (2012) Evolution of middle to Late Cretaceous oceans- A 55 m.y. record of Earth's temperature and carbon cycle. *Geology*, **40**, 107-110.

Francis, J.E. and **Frakes, L.A.** (1993) Cretaceous climates. In: *Sedimentology Review/1* (Ed. V. P. Wright) pp. 17-31. Blackwell Scientific Publications, Oxford.

Francus, P., Bradley, R.S. and **Thurow, J.W.** (2004) An introduction to image analysis, Sediments and Paleoenvironmnets. In *Image Analysis, Sediments and Paleoenvironments* (Ed. P. Francus) pp. 1-11. Kluwer Academic Publishers, Dordrecht.

Garrett, C. (2003) Internal Tides and Ocean Mixing. *Science*, **301**, 1858-1859.

Grippo, A., Fischer, A.G., Hinnov, L.A., Herbert, T.D. and **Silva, I.P** (2004) Cyclostratigraphy and chronology of the Albian Stage (Piobbico core, Italy). In: Cyclostratigraphy: *Approaches and Case Histories* (Eds. B. D'Argenio, A.G.Fischer, I.P. Silva, H. Weissert, V. Ferreri), SEPM Special Publication, **81**, 57-81.

Haq, B.U., Hardenbol, J and **Vail, P.R.** (1988) Mesozoic and Cenozoic chronostratigraphy and eustatic cycles. In: Sea-level Change: an Integrated Approach (Eds. C.K. Wilgus, B.S Hastings, C.G. Kendall, H.W. Posamentier, H.W. Ross, J.C. Van Wagoner), *SEPM special publication*, 42, 71-108.

Hancock, J.M. and **Kauffman, E.G.** (1979) The great transgressions of the Late Cretaceous. *Journal of the Geological Society, London*, **136**, 175-186.

Hay, W.W. (2008) Evolving ideas about the Cretaceous climate and ocean circulation. *Cretaceous Research*, **29**, 725-753.

Hay, W.W. and **Floegel, S.** (2012) New thoughts about the Cretaceous climate and oceans. *Earth-Science Reviews*, **115**, 262-272.

Hasegawa, H., Tada, R., Jiang, X., Suganuma, Y., Imsamut, S., Charusiri, P., Ichnnorov, N. and **Khand, Y.** (2011) Drastic shrinking of the Hadley circulation during the mid-Cretaceous supergreenhouse. *Climate of the Past Discussions*, **7**, 119-151.

Herčík, F., Hermann, Z. and **Valečka, J.** (1999) Hydrogeologie české křídové pánve.ČGS, Praha. 115 pp.

Hinnov, L.A. (2000) New Perspectives on Orbitally Forced Stratigraphy. *Annual Rev. Earth Planet. Sci*., **28**, 419-475.

Hrouda, F. (1994) A technique for the measurement of thermal changes of magnetic susceptibility of weakly magnetic rocks by the CS-2 apparatus and KLY-2 Kappabridge. *Geophys. J. Int*., **118**, 604-612.

Hrouda, F. (2010) Modelling Relationship Between Bulk Susceptibility and AMS in Rock Consisting of Two Magnetic Fractions Represented by Ferromagnetic and Paramagnetic Minerals – Implications for Understanding Magnetic Fabrics in Deformed Rocks, *Journal Geological Society of India*, **75**, 254-266.

Hrouda, F., Chlupáčová, M. and **Chadima, M.** (2009) The Use of Magnetic Susceptibility of Rocks in Geological Exploration (case histories study). Leaflet of Georadis s.r.o, Brno, 29 pp.

Hrouda, F. and **Kahan, Š.** (1991) The magnetic fabric relationship between sedimentary and basement nappes in the High Tatra Mts. (N Slovakia). *J. Struct. Geol*., **13**, 431-442.

Hu, X., Wagreich, M. and **Yilmaz, I.O.** (2012) Marine rapid environmental/climatic change in the Cretaceous greenhouse world. *Cretaceous Research*, **38**, 1-6.

Jarvis, I., Gale, A.S., Jenkyns, H.C. and **Pearce, M.A** (2006) Secular variation in Late Cretaceous carbon isotopes: a new delta C-13 carbonate reference curve for the Cenomanian-Campanian (99.6-70.6 Ma). *Geological Magazine*, **143**, 561-608.

Jarvis, I., Murphy, A.M. and **Gale, A.S.** (2001) Geochemistry of pelagic and hemipelagic carbonates: criteria for identifying systems tracts and sea-level change. *Journal of the Geological Society, London*, **158**, 685-696.

Jones, C.E. and **Jenkyns, H.C.** (2001) Seawater strontium isotope, oceanic anoxic events, and seafloor hydrothermal activity in the Jurassic and Cretaceous. *American Journal of Science,* **301**, 112-149.

Koptíková, L., Bábek, O., Hladil, J., Kalvoda, J. and **Slavík, L.** (2010) Stratigraphic significance and resolution of spectral reflectance logs in Lower Devonian carbonates of the Barrandian area,

Czech Republic; a correlation with magnetic susceptibility and gamma-ray logs. *Sedimentary Geology*, **225**, 83-98.

Košťák, M., Čech, S., Ekrt, B., Mazuch, M., Wiese, F., Voigt, S., and **Wood, C.J.** (2004) Belemnites of the Bohemian Cretaceous Basin in a global context. *Acta Geologica Polonica 54*, **4**, 511-533.

Kößler, P., Herrle, J.O., Appel, E., Erbacher, J. and **Hemleben, C.** (2001) Magnetic records of climatic cycles from mid-Cretaceous hemipelagic sediments of the Vocontian Basin, SE France. *Cretaceous Research*, **22**, 321-331.

Krutský, N., Váně, M., Holá,A. and **Hercogová, J.** (1975) Turon and coniak v dolním Poohří. *Sborník geologických věd, Geologie*, **27**, 99-142.

Lamoureux, S.F. and **Bollmann, J.** (2004) Image Acquisition. In *Image Analysis, Sediments and Paleoenvironments* (Ed. P. Francus) pp. 11-35. Kluwer Academic Publishers, Dordrecht.

Larson, R.L. (1991) Latest pulse on Earth: Evidence for a mid-Cretaceous superplume. *Geology*, **19**, 547-550.

Laurin, J. (in prep.) Towards understanding the signature of riverine siliciclastic input in hemipelagic strata: Ti/Al ratios. To be submitted to *Geology.*

Laurin, J., Čech, S., Uličný, D., Štaffen, Z., Svobodová, M. (in prep.) An orbital time scale for the Upper Turonian: on the timing of carbon-cycle perturbations at the demise of peak greenhouse. To be submitted to *Earth and Planetary Science Letters*.

Laurin, J. and **Uličný, D.** (2004) Controls on a shallow-water hemipelagic carbonate system adjacent to a siliciclastic margin: example from Late Turonian of central Europe. .*Journal of Sedimentary Research*, **74**, 697-717.

Laurin, J. and **Vodrážka, R.** (2010) Record of sea-level fall in shallow-water hemipelagic strata: case study and numerical modelling. *Terra Nova*, **22**, 103-109.

Lurcock , P.C. and **Wilson G.S.** (in press) The Paleomagnetism of glauconitic sediments. *Global and Planetary Change*.

MacEachern, J.A., Pemberton, S.G., Gingras, M.K. and **Bann, K.L.** (2010) Ichnology and facies models. In: *Facies Models* (Eds. R.W. Dalrymple, N.P. James) 4th Edition, pp. 19-58. Geological Association of Canada, St.Johns.

Malkovský, M. (1974) Tektonický vývoj území české křídové pánve. In: *Geologie české křídové pánve a jejího podloží* (Ed. J. Svoboda) pp. 12-25 and 116-131. Ústřední ústav geologický, Praha.

Malkovský, M. (1987) The Mesozoic and Tertiary basins of the Bohemian Massif and their evolution. *Tectonophysics*, **137**, 31-42.

Mann M.E. and **Lees J.M.** (1996) Robust Estimation of Background Noise and Signal Detection in Climatic Time Series. *Climatic Change*, **33**, 409-445.

Mayer, H. and **Appel, E.** (1999) Milankovitch cyclicity and rock-magnetic signatures of palaeoclimatic change in the Early Cretaceous Biancone Formation of the Southern Alps, Italy. *Cretaceous Research*, **20**, 189-214.

Meyers, S.R., Sageman, B.B., and **Hinnov, L.A.** (2001) Integrated quantitative stratigraphy of the Cenomanian-Turonian Bridge Creek Limestone Member using evolutive harmonic analysis and stratigraphic modeling. *Journal of Sedimentary Research* , **71**, 628–643.

Meyers, S.R. and **Sageman, B.B**. (2007) Quantification of deep-time orbital forcing by average spectral misfit.. *American Journal of Science*, **307**, 773-792.

Miller, K.G., Kominz, M.A., Browning, J.V., Wright, J.D., Mountain, G.S., Katz, M.E., Sugarman, P.J., Cramer, B.S., Christie-Blick, N. and **Pekar, F.** (2005) The Phanerozoic Record of Global Sea-Level Change. *Science*, **310**, 1293-1297.

Miller, K.G, Sugarman, P.J., Browning, J.V., Komnitz, M.A., Hernández, J.C., Olsson, R.K., Wright, J.D., Feigenson, M.D. and **Sickel, W.V.** (2010) Late Cretaceous chronology of large, rapid sea-level changes: Glacioeustasy during the greenhouse world. *Geology*, **7**, 585-588.

Mitchell, A.J., Uličný, D., Hampson, G.J., Allison, P.A., Gorman, G.J., Piggott, M.D., Wells, M.R. and **Pain, C.C.** (2010) Modelling tidal current-induced bed shear stress and palaeocirculation in an epicontinental seaway: the Bohemian Cretaceous Basin, Central Europe. *Sedimentology*, **57**, 359-388.

Munk, W., Dzieciuch, M. and **Jayne, S.** (2002) Millennial Climate Variability: Is There a Tidal Connection? *Journal of Climate*, **15**, 370-385.

Nichols, G. (2009) Sedimentology and Stratigraphy. 2nd edn. Wiley-Blackwell, Chichester, 432 pp.

Nederbragt, A.J. and **Thurow, J.W.** (2004) Digital sediment colour analysis as a method to obtain high resolution climate proxy records. In *Image Analysis, Sediments and Paleoenvironments* (Ed. P. Francus) pp. 105-125. Kluwer Academic Publishers, Dordrecht.

Ortiz, J.D. and **O'Connell, S.** (2004) Toward a non-linear grayscale calibration method for legacy photographic collections. In *Image Analysis, Sediments and Paleoenvironments* (Ed. P. Francus) pp. 125-143. Kluwer Academic Publishers, Dordrecht.

Paillard, D., Labeyrie, L. and **Yiou, P**. (1996) Macintosh program performs time-series analysis, Eos (Transactions, American Geophysical Union) 77: 379 *zkontrolovat na netu*

Pek, I. and **Mikuláš, R.** (1996) Úvod do studia fosilních stop. Český geologický ústav, Praha, 30 pp.

Pokorný, J., Pokorný, P., Suza, P. and **Hrouda, F.** (2011) A Multi-Function Kappabridge for High Precision Measurement of the AMS and the Variations of Magnetic Susceptibility with Field, Temperature and Frequency. In: *The Earth's Magnetic* Interior (Ed. E. Petrovský, E. Herrera-Bervera, T. Harinarayana, D. Ivers) pp. 293-294. Springer, Berlin.

Porter, S.C. (2000) High-Resolution Paleoclimatic Information from Chinese Eolian Sediments based on Grayscale Intensity Profiles. Quaternary Research, **53**, 70-77.

Rotnicka, J. (2005) Ichnofabrics of the Upper Cretaceous fine-grained rocks from the Stolowe Mountains (Sudetes, SW Poland). *Geological Quarterly*, **49**, 15-30.

Sageman, B.B. and **Lyons, T.W.** (2004) Geochemistry of Fine-grained Sediments and Sedimentary Rocks. In: *Sediments, Diagenesis, and Sedimentary Rocks* (Ed. F.T. Mackenzie) pp. 115-158. Elsevier Publ., New York.

Schallreuter, R. (1984) Framboidal Pyrite in deep-sea sediments. In: *Initial Report Deep Sea Drilling Project* , **75**, 875-891.

Schlanger, S.O. and **Jenkyns H.C.** (1976) Cretaceous Oceanic Anoxic Events: Causes and Consequences. *Geologie en mijnbouw*, 55, 179-184.

Scholle, P.A. (1978) A Color Illustrated Guide to Carbonate Rock Constituents, Textures, Cements, and Porosities: AAPG Memoir 27. The American Association of Petroleum Geologists, Tulsa, 241 pp.

Scholle, P.A. (1979) A Color Illustrated Guide to Constituents, Textures, Cements, and Porosities of Sandstones and Associated Rocks: AAPG Memoir 28. The American Association of Petroleum Geologists, Tulsa, 201 pp.

Scholle, P.A. and **Ulmer-Scholle, D.S.** (2003) A Color Guide to the Petrography of Carbonate Rocks: Grains, textures, porosity, diagenesis: AAPG Memoir 77. The American Association of Petroleum Geologists, Tulsa, 474 pp.

Schwarzacher, W. (1993) Cyclostratigraphy and the Milankovitch Theory. Elsevier, London, 221 pp.

Skoček, V. and **Valečka, J.** (1983) Palaeoeography of the Late Cretaceous Quadersandstein of central Europe. *Palaeogeography, Palaeoclimatology, Palaeoecology*, **44**, 71-92.

Sokolova, E.A. (2009) Early Turonian Global Warming in the Atlantic and Indian Oceans According to the Data of the Foraminifera Analysis. *Oceanology***, 49**, 681-687.

Stage, M. (2001) Magnetic susceptibility as carrier of a climatic signal in chalk. *Earth and Planetary Science Letters*, **188**, 17-27.

Štaffen, Z. (1999) Chemostratigrafické stanovení ekvivalence vrstev a souvrství české křídové pánve. *Acta Musei Richnoviensis, Sect. Nature. 6*, **2**, 1-153.

Thomson, D.J. (1982) Spectrum estimation and harmonic analysis. Proceedings of the IEEE, 70, 1055-1096.

Tyson, R.V. and **Funnell, B.M.** (1987) European Cretaceous shorelines, stage by stage. *Paleogeography, Palaeoclimatology, Palaeoecology*, **59**, 69-91.

Tucker, M.E. (2001) Sedimentary Petrology: An Introduction to the Origin of Sedimentary Rocks. 3rd edn. Blackwell Science, Oxford, 262 pp.

Uličný, D. (2001) Depositional systems and sequence stratigraphy of coarse-grained deltas in a shallow-marine, strike-slip setting: the Bohemian Cretaceous Basin, Czech Republic. *Sedimentology*, **48**, 599-628.

Uličný, D., Čech, S. and **Grygar, R.** (2003) Tectonics and depositional systems of a shallow-marine, intra-continental strike-slip basin: exposures in Český Ráj region, Bohemian Cretaceous Basin. In: *Excursion Guide, First Meeting of the Central European Tectonics Group and Eighth meeting of the Czech Tectonics Studies Group. Geolines*, **16**, 133-148.

Uličný, D., Gröcke, D., Čech, S., Laurin, J., Jarvis, I., Olde, K., Trabucho-Alexandre, J., Švábenická, L., Pedentchouk, N. and **Grygar, T.M.** (submitted) High-resolution carbon-isotope record of the Turonian stage correlated to a siliciclastic basin fill: implications for mid-Cretaceous sea-level changes. *Palaeogeography,Palaeoclimatology,Palaeoecology*.

Uličný, D., Laurin, J. and **Čech, S.** (2009) Controls on clastic sequence geometries in a shallow-marine, transtensional basin: the Bohemian Cretaceous Basin, Czech Republic. *Sedimentology*, **56**, 1077-1114.

Uličný, D. and **Špičáková, L.** (1996) Response to high-frequency sea-level change in a fluvial to estuarine succession: Cenomanian paleovalley fill, Bohemian Cretaceous Basin. In: *High resolution Sequence Stratigraphy: Innovations and Applications* (Eds J.A. Howell and J.F. Aitken), Geol. Soc. Spec. Publ., **104**, 247-268.

Valečka, J. (1979) Paleogeografie a litofaciální vývoj severozápadní části české křídové pánve. *Sborník geologických věd, Geologie*, **33**, 47-81.

Valečka, J. and **Skoček, V.** (1990) Late Cretaceous lithoevents in the Bohemian Cretaceous Basin, Czechoslovakia. Cretaceous Research, 12, 561-577.

Voigt, S., Wagreich, M., Surlyk, F., Walaszczyk, I., Uličný, D., Čech, S., Voigt, T., Wiese, F., Wilmsen, M., Niebehr, B., Reich, M., Funk, H., Michalík, J., Jagt, J.W.M., Felder, P. J. and **Schulp, A.S.** (2008) Cretaceous. In: *Geology of Central Europe, Volume 2:Mesozoic and Cenozoic* (Ed. T. McCann) p. 923-997. The Geological Society, London.

Voigt, S. and **Wiese, F.** (2000) Evidence for late Turonian (Late Cretaceous) climate cooling Oxygen isotope variations and paleobiogeographic changes in Western and Central Europe. *Journal of the Geological Society, London*, **157**, 737-744.

Weedon, G.P. (2003) Time-Series Analysis and Cyclostratigraphy Examining stratigraphic records of environmental cycles. Cambridge University Press, Cambridge. 260 pp.

Wiese, F., Čech, S., Ekrt, B., Košťák, M., Mazuch, M and **Voigt, S**. (2004) The Upper Turonian of the Bohemian Cretacceous Basin (Czech Republic) exemplified by the Úpohlavy working quarry: integrated stratigraphy and palaeoceanography of a gateway to the Tethys. *Cretaceous Res*., **25**, 329-352.

Zabel, M., Bickert, T. and **Dittert, L.** (1999) Significance of the sedimentary Al:Ti ratio as an indicator for variations in the circulation patterns of the equatorial North Atlantic. *Paleoceanography*, **14**, 789-799.

Ziegler, P.A. (1990) Geological Atlas of Western and Central Europe. Shell International Petroleum Maatschapij, The Hague, 239 pp.

8 Appendix

This is a selected list of appendices; these are the most informative or have been evaluated as critical to the text. A number of other supporting information is attached on the accompanying CD.

8.1 List of printed appendices

Appendix 1 Information on the Bch-1 core

Appendix 2 Geochemistry calibrations

Appendix 3 Magnetic Susceptibility calibration

Appendix 4 Sedimentation rate model

8.2 List of CD content

Appendix 1 Information on the Bch-1 core

Appendix 2 Geochemistry calibrations

Appendix 3 Magnetic Susceptibility calibration

Appendix 4 Sedimentation rate model

Appendix 5 EHA of magnetic susceptibility and grayscale

Appendix 6 Sample positions

Appendix 7 Frequency dependent MS

Appendix 1. Information on the Bch-1 core

This project was funded by grant GACR grant number P210/10/1991 Principal Investigator RNDr D. Uličný CSc.

The Bch-1 drill site is positioned at 50°18´54.2´´N and 15°17´42.03´´E, the core reached 405 m. The lithology was originally described by Mgr. S. Čech and RNDr. D. Uličný, CSc. The core was drilled by the wireline technique and is six centimetres in diameter, with a recovery rate exceeding 90 %.

Fig. Ap.1
The washed core as photographed for the purposes of grayscale extraction. One of the light coloured Lithotype III beds displayed as well as a bioclastic fragment above. Note the almost imperceptible hairline crack between the two separate peaces; this was the case for most of the core allowing for an acquisition of unbroken grayscale record.

Appendix 2. Geochemistry Calibrations

Calibration equations of XRF geochemistry datasets are courtesy of Mgr. Jiří Laurin, Ph.D.

Dataset 1:

XRF analysis performed at the Institute of Inorganic Chemistry, AS CR; calibration equations supplied by the Institute of Inorganic Chemistry, AS CR

Al_{CAL} (wt.%) = -0.0000789*(Al_{XRF} ^2) + 0.044* Al_{XRF} - 0.244

Si_{CAL} (wt.%) = 0.0261* Si_{XRF} - 0.5447

Ca_{CAL} (wt.%) = -0.00000001*(Ca_{XRF} ^2) + 0.0018* Ca_{XRF} + 1.3985

Ti_{CAL} (wt.%) = -0.0000039*(Ti_{XRF} ^2) + 0.0021* Ti_{XRF}

Zr_{CAL} (wt.%) = -0.000000155*(Zr_{XRF} ^2) + 0.000201* Zr_{XRF}

Dataset 2:

XRF analysis performed at the Institute of Geophysics, AS CR, using a handheld XRF analyzer. Zr, Ti and Al calibrations based on ICP MS analysis (SGS, Toronto), Ca and Si calibrated with the classical silicate-rock analysis (Geological Survey, Prague).

Zr_{CAL} (wt.%) = 0.0009*(Zr_{XRF} ^2) + 0.4593* Zr_{XRF}

Al_{CAL}(wt.%)=0.0418*(Al_{XRF}^2)+0.8454*Al_{XRF}

Ti_{CAL} (wt.%) = -1.242*(Ti_{XRF} ^2) + 1.238* Ti_{XRF}

Ca_{CAL} (wt.%) = -0.0058*(Ca_{XRF} ^2) + 0.8607* Ca_{XRF} + 6.5568

Si_{CAL} (wt.%) = 0.0091*(Si_{XRF} ^2) + 0.2523* Si_{XRF} + 5.4067

Appendix 3. Kappameter calibration

The Kappameter dataset has proven different in value to Kappabridge measurements; this is to some degree unresolved as both devices should give the same value. The difference probably lies in the automatic core correction or a wrong entry of the diameter value. The Kappabridge dataset appears to be more precise and they were taken as a standard; fortunately the relationships between both methods are strictly linear, see **fig. Ap.4,** therefore a simple re-calculation was adopted.

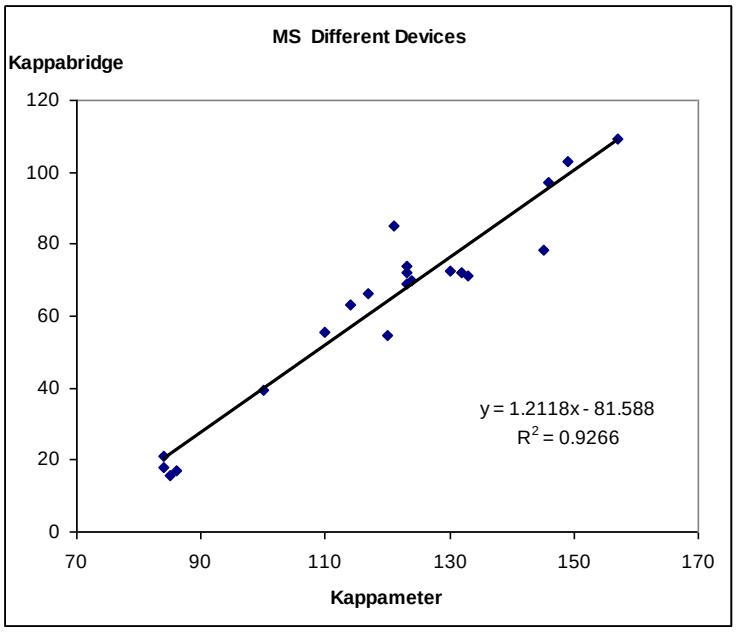

Fig. Ap.4
Showing correlation between the 21 correction samples and their counterparts in the Kappameter series showing a good correlation, however the data do display different MS as can be seen from the x and y axis values, The ensuing procedure therefore was to reduce the value of original log based on the equation of linear regression.

Equation:

The value of coefficient of determination for linear least square regression is 0.93 which is considered a very good fit (*e.g. Mayer & Appel, 1999*). The mismatch in total MS value was probably caused by discrepancies connected to the core size correction.

Appendix 4. Sedimentation rate model

Sedimentation rate estimates were calculated using the biostratigraphic and carbon-isotope markers, see **Tab.Ap.5**. Some of them have been pinpointed on the core, others have been correlated from the surrounding cores (marked in red colour). The floating time scale has been incorporated from Laurin et al. (*in prep.*)

Tab.Ap.5

This table shows biostratigraphic and carbon-isotope markers with their assigned floating time-scale value

Marker	Floating time scale [kyr]
FO C. crassus	-241
Navigation Event	0
Did I	130
FO P. germari	340
FO M. scupini	705
Bridgewick Event	1255
FO I.perplexus	1459
Pewsey Event	1500
Glynde Event	1788

The resultant sedimentation rate model is shown on the **fig. A.5,** which shows the intervals between two consecutive markers and the calculated sedimentation rate (dark blue lines) plus a model situation where continuous sedimentation without major jumps in sedimentation Rate is expected (aqua colour trend).